Accepted Manuscript

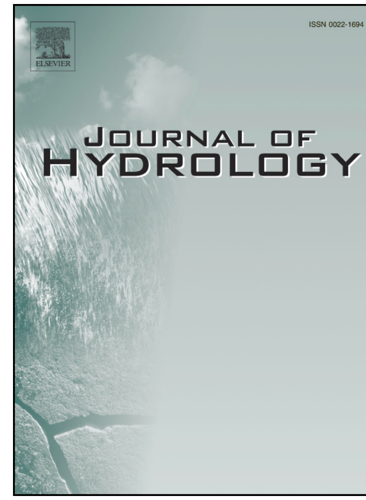

Investigating summer flow paths in a Dutch agricultural field using high frequency direct measurements

J.R. Delsman, M.J. Waterloo, M.M.A. Groen, J. Groen, P.J. Stuyfzand

PII: S0022-1694(14)00853-1
DOI: http://dx.doi.org/10.1016/j.jhydrol.2014.10.058
Reference: HYDROL 20008

To appear in: *Journal of Hydrology*

Received Date: 11 July 2014
Revised Date: 22 October 2014
Accepted Date: 27 October 2014

Please cite this article as: Delsman, J.R., Waterloo, M.J., Groen, M.M.A., Groen, J., Stuyfzand, P.J., Investigating summer flow paths in a Dutch agricultural field using high frequency direct measurements, *Journal of Hydrology* (2014), doi: http://dx.doi.org/10.1016/j.jhydrol.2014.10.058

Investigating summer flow paths in a Dutch agricultural field using high frequency direct measurements

Journal of Hydrology

J.R. Delsman [a,b] joost.delsman@deltares.nl

M.J. Waterloo [b] m.j.waterloo@vu.nl

M.M.A. Groen [b] m.m.a.groen@vu.nl

J. Groen [b,c] koos.groen@acaciawater.com

P.J. Stuyfzand [b,d] pieter.stuyfzand@kwrwater.nl

[a] Department of Soil and Groundwater, Deltares, Utrecht, Netherlands

PO Box 85467, 3508 AL Utrecht, Netherlands

[b] Critical Zone Hydrology Group, Department of Earth Sciences, VU University Amsterdam, Amsterdam, Netherlands

De Boelelaan 1085, 1081 HV Amsterdam, Netherlands

[c] Acacia Water, Gouda, Netherlands

Jan van Beaumontstraat 1, 2805 RN Gouda, Netherlands

[d] KWR Watercycle Research Institute, Nieuwegein, Netherlands

P.O. Box 1072, 3430 BB Nieuwegein, Netherlands

Corresponding author

J.R. Delsman

Deltares

PO Box 85467

3508 AL Utrecht

Netherlands

joost.delsman@deltares.nl

+31 6 30548980

ACCEPTED MANUSCRIPT

Abstract

The search for management strategies to cope with projected water scarcity and water quality deterioration calls for a better understanding of the complex interaction between groundwater and surface water in agricultural catchments. We separately measured flow routes to tile drains and an agricultural ditch in a deep polder in the coastal region of the Netherlands, characterized by exfiltration of brackish regional groundwater flow and intake of diverted river water for irrigation and water quality improvement purposes. We simultaneously measured discharge, electrical conductivity and temperature of these separate flow routes at hourly frequencies, disclosing the complex and time-varying patterns and origins of tile drain and ditch exfiltration. Tile drainage could be characterised as a shallow flow system, showing a non-linear response to groundwater level changes. Tile drainage was fed primarily by meteoric water, but still transported the majority (80%) of groundwater-derived salt to surface water. In contrast, deep brackish groundwater exfiltrating directly in the ditch responded linearly to groundwater level variations and is part of a regional groundwater flow system. We could explain the observed salinity of exfiltrating drain and ditch water from the interaction between the fast-responding pressure distribution in the subsurface that determined groundwater flow paths (wave celerity), and the slow-responding groundwater salinity distribution (water velocity). We found water demand for maintaining water levels and diluting salinity through flushing to greatly exceed the actual sprinkling demand. Counterintuitively, flushing demand was found to

be largest during precipitation events, suggesting the possibility of water savings by operational flushing control.

Keywords

Groundwater – surface water interaction; direct measurements; flow separation; agricultural field; salinization

Highlights

- We physically separated and measured flow paths to an agricultural ditch
- High frequency measurements revealed dynamic origin of drain and ditch outflow
- Tile drains transport the majority of groundwater-derived salts to surface water
- Salinity variations explained by interaction of water velocity and wave celerity
- Surface water flushing demand was found to greatly exceed sprinkling demand

Abbreviations

BSL – Below mean Sea Level

BGS – Below Ground Surface

EC – Electrical conductivity

TDS – Total Dissolved Solids

SW-GW – Surface water – groundwater

CVES – Continuous Vertical Electrical Sounding

1 Introduction

Delta areas are hotspots for human settlement and agriculture, owing to their fertile soils, low relief and easy transport connections (Aerts et al., 2009). Delta areas also pose specific challenges related to flood risks, infrastructure construction in unconsolidated sediments, and salt water intrusion threatening fresh groundwater resources (Custodio and Bruggeman, 1987). In many deltas groundwater table lowering, resulting from artificial drainage, causes an upward flow of brackish and nutrient rich groundwater, with adverse effects on surface water quality (De Louw et al., 2011b). Exfiltration of brackish groundwater is a major concern in low-lying polder areas in the Netherlands and is generally mitigated by diluting the surface water system with diverted river water (Van Rees Vellinga et al., 1981). The prospect of decreasing river discharges (Forzieri et al., 2014) and hence increasing water shortages has, however, prompted Dutch water managers to seek alternative strategies and minimize the intake of diverted river water (Delta Programme Commissioner, 2013). Alternative strategies require detailed knowledge of the flow of water and solutes in these areas, specifically regarding the exfiltration of brackish groundwater and the fate of diverted river water during summer periods.

Polders are artificially drained, embanked tracts of low elevated land that originated as reclaimed lakes, embanked floodplains or embanked and drained marshlands and are common throughout the coastal zone of the Netherlands (Schultz, 1992). Polders are intensively drained by tile drains and ditches, and agriculture is generally the dominant landuse. Polder surface water levels are maintained within narrow limits by pumping excess water, consisting of both precipitation excess and exfiltrating regional groundwater flow, onto the “boezem”, a receiving system of canals. In summer, diverted river water is transported by the boezem and taken in by polders via weirs or inlet culverts to supplete precipitation deficits and, as already noted, flush the surface water system to mitigate the adverse effects of exfiltrating brackish groundwater (Van Rees Vellinga et al., 1981).

Hydrological and chemical catchment response is a reflection of the wide variety of flow routes followed by water droplets entering surface water, each acquiring a distinct chemical signature along its route (Sophocleous, 2002). The linkage between flow routes and hydrological response is most direct in headwater streams or ditches, where interaction between surface water and its surroundings is highest. Headwater streams have therefore always been prime focus areas of hydrological study (Sophocleous, 2002). Encouraged by the recent IAHS “Panta Rhei” initiative (Montanari et al., 2013), focusing hydrological research on change in hydrology and society, attention has shifted somewhat away from pristine natural catchments to actively managed agricultural catchments. While some studies report emerging linear and thus simpler behavior (Basu et al., 2010), both profound modifications to natural hydrologic functioning and intermittent direct human impacts complicate the hydrologic and chemical response of actively managed agricultural catchments (Montanari et al., 2013; Rozemeijer and Broers, 2007).

In polder and other low-land agricultural catchments, tile drains are a major pathway for exfiltrating groundwater and associated solutes (De Louw et al., 2013; Kennedy et al., 2012; Rozemeijer et al., 2010; Tiemeyer et al., 2006; Van der Velde et al., 2010b; Velstra et al., 2011). The importance of tile drains is irrespective of whether solutes originate from agricultural practices at the ground surface or from regional groundwater exfiltration, the dominant source of solutes in Dutch polders (Griffioen et al., 2013). With solutes originating from the ground surface, groundwater flow to an agricultural ditch was found to only be a significant transport route after tile drains had run dry during summer periods (Rozemeijer et al., 2010). For a site where solutes originated from regional groundwater flow, Van den Eertwegh (2002) estimated, based on mixing equations, groundwater flow to agricultural ditches to account for between 20 and 50% of annual chloride loads. In selected polders boils, localized preferential seepage pathways intersecting a low-permeable confining layer (De Louw et al., 2010), form a dominant solute pathway. Boils may contribute up to 60% (De Louw et al., 2011b) or 80% (Delsman et al., 2013) of exfiltrated solutes. The fate of diverted irrigation water understandably received much attention in irrigation schemes in arid regions (e.g., Kahlown and Kemper, 2004), but few studies attempted to attribute water loss from drainage channels to either groundwater infiltration or evaporation (e.g., Bosman, 1993). While water shortages and water quality deterioration are also a factor in more humid climates, we know of no studies that measured and attributed water loss in these climates. Rozemeijer et al. (2012) traced the propagation of diverted river water in an agricultural polder catchment in the Netherlands and found diverted river water to follow short-circuit flow routes, never reaching headwater ditches. Delsman et al. (2013) investigated flow routes in an agricultural deep polder catchment using environmental tracers, revealing relatively constant contributions of regional groundwater and diverted river water, while tile drain flow dominated discharge events.

No study, however, comprehensively studied all incoming and outgoing flow routes in an agricultural polder catchment receiving inputs from both regional groundwater flow and diverted river water. Moreover, water (and solute) balance terms that are generally considered unimportant in humid climates may prove important in understanding catchment behaviour in dry summer periods. This understanding is crucial to outline management strategies that focus on mitigating the effects of increasing water shortages and deteriorating water quality in agricultural areas. This paper therefore specifically focuses on the growing season and investigates (1) flow routes of precipitation and brackish regional groundwater to tile drains and headwater ditches, including the fate of diverted river water, (2) resulting surface water solute dynamics, and (3) implications for water management, on both seasonal and event scales. To this end we physically separated and measured tile drain and ditch flow routes of water and associated solutes in a representative agricultural field in the coastal region of the Netherlands during the meteorologically different 2012 and 2013 growing seasons.The significant salinity contrast between precipitation and brackish regional groundwater allowed detailed geophysical mapping of their subsurface distributions and relatively easy computation of the regional groundwater contribution in measured water fluxes.

2 Materials and methods

2.1 Study area

We studied the interaction between a ditch and a 900 m x 125 m agricultural field in the Schermer polder, located 20 km north of Amsterdam, the Netherlands (52.599° N, 4.782° E) (Figure 1). The Schermer polder is a former fresh water lake (48 km^2) reclaimed in 1635 AD. Average yearly precipitation and Makkink reference evaporation (Makkink, 1957) amount to 880 mm and 590 mm respectively. Relief is essentially flat at a surface elevation of 4.0 (± 0.14) m below mean sea level (BSL). The field is drained with tile drains, installed at a depth of 1.0 m below ground surface (BGS) at 5 m intervals, and ditches on both sides of the field. Tile drains discharge in the northern ditch, in which the surface water level was maintained at a constant 5.0 m BSL with a pump, whereas the water level in the southern ditch was maintained at 4.7 m BSL. Potatoes and lettuce were grown on the field for the first and second year of study, respectively.

Geohydrology of the area is characterized by Holocene marine deposits of the Naaldwijk formation, consisting of marine clays to loamy to coarse sands (Weerts et al., 2005). Shallow 2 m corings on the field revealed a consistent 20 – 40 cm thick tillaged clay layer on top of fairly homogeneous loamy sand. This sandy layer extends to a depth of at least 17 m, as evidenced by an existing coring on the western end of the field. The Naaldwijk formation extends to 20 m BGS, where it overlies a thick aquifer of fluvial sands of the Kreftenheye and Urk formations (Weerts et al., 2005). Regional groundwater flows in an easterly direction and belongs to a system with infiltration in the coastal dune area to the west of the study area and exfiltration in the Schermer polder. Groundwater in the area is brackish to saline (around 5 g/l Cl), as a result of free convection during marine transgressions around 5000 y BC (Delsman et al., 2014; Post et al., 2003). The hydraulic gradient at the study area ensures a constant upward groundwater flow, estimated at 0.5 mm/day (I.C.W., 1982). The corresponding exfiltration of brackish to saline groundwater adversely affects surface water quality. The annual precipitation excess ensures the development of shallow rainwater lenses (De Louw et al., 2011a) on top of the upward flowing brackish groundwater flow, which allows for the cultivation of salt-sensitive crops. Boils, preferential pathways for exfiltrating groundwater (De Louw et al., 2010), were not present at the field site.

Water management in the Schermer polder is exemplary for polders in the Netherlands.Surface water levels are maintained at a constant level, by pumping out excess water in wet periods and taking in diverted river water when evaporation rates exceed precipitation and groundwater inflow. During the growing season (Apr – Oct) the polder drainage system is continuously flushed with additional diverted fresh river water to dilute the saline groundwater input into the drainage system. The ditch on the southern end of the field is in open connection with the main canal and receives this diverted river water, the northern ditch does not. The average amount of diverted river water use was estimated at 0.4 mm/d (0.7 mm/d in summer) over the entire Schermer polder area (Oosterwijk, 2009).

Figure 1

2.2 Measurement setup

To allow separate measurements of both tile drain fluxes and groundwater flux directly into a ditch, we isolated a 35 m stretch of ditch by inserting two steel bulkheads down to a depth of 1 m below ditch bottom. The bulkheads were connected by a 160 mm diameter tube to act as a culvert for the rest of the ditch (Figure 1, Figure 2). The bulkheads were each placed exactly between two tile drains, such that a groundwater divide extended from the barriers across the agricultural field. As both surface water level and groundwater head differences between both sides of the barriers were minimal, we assumed fluxes across these boundaries to be negligible. In this isolated ditch stretch, all seven tile drains were interconnected and flowed out into a 100 L reservoir positioned in the ditch bank (reservoir 1 in Figure 1). Water was intermittently pumped out of this reservoir, maintaining free outflow conditions. Discharge was measured using a digital turbine flow meter (MSD Cyble, Itron, France) and electrical conductivity (EC) in the reservoir was registered at 15 min intervals (CTD-Diver, Schlumberger, Netherlands). We installed two additional 100 L reservoirs to allow measurement of both incoming and outgoing water fluxes to and from the ditch. The ditch flowed out into reservoir 3 (through a filter to prevent pump clogging), containing a pump to provide a small constant flux back into the ditch, and an overflow into reservoir 2. In a water-surplus situation net inflow into reservoir 1 was positive and flowed out into reservoir 2, where it was pumped out and measured. In a water-shortage situation however, net inflow into reservoir 1 was negative and caused a water level drop, triggering the inflow of external water, representing diverted river water, into reservoir 1 and subsequently into the isolated ditch stretch. Quantity and EC of both in- and outgoing water fluxes were measured analogously to the tile-drainage setup.

Groundwater heads were measured in two adjacent piezometers screened at 0.8 – 1.0 m and 1.8 – 2.0 m BGS, at 9 locations perpendicular to the ditch both at and between tile drain locations. Groundwater heads below the ditch were measured in a piezometer located in the centre of the ditch, screened at 2.55 – 2.75 m below ditch bottom, an additional piezometer screened at 1.8 – 2.0 m BGS measured groundwater heads on the roadside of the ditch. Piezometers were equipped with automated pressure and temperature loggers (Diver, Schlumberger, Netherlands) and measured at 15 min intervals. ECs were recorded in nine shallow-screened piezometers, and the piezometer screened at 2.55 – 2.75 m below the ditch bottom (CTD-Diver). We transformed measured point water heads to equivalent freshwater heads (Post et al., 2007). For brevity, we refer to equivalent freshwater heads as groundwater heads throughout the remainder of this paper. Piezometers were concentrated around the ditch; the furthest piezometers are located only 6 meters from the ditch bank. We opted for this setup to minimally interrupt day-to-day agricultural use of the field, while the narrow tile drain spacing will ensure an only limited zone-of-influence of the ditch. Ditch water level and EC were measured at 15 min intervals using a pressure sensor in a stilling well located in the centre of the ditch (CTD-diver; from Oct 2012 onwards also by a Unik 5000, General Electric, Germany). We used a straightforward Kalman-filtering approach, based on reported sensor variances (Table 1), to combine the two ditch water level measurements and minimize the resulting uncertainty. We installed soil moisture sensors (CS616, Campbell Scientific, USA) at 6 m from the ditch bank, both at and between tile drains, at 10, 25, 50 and 85 cm BGS, and calibrated for the encountered soil types. Groundwater temperature was measured around the ditch – field interface with five temperature sensor arrays perpendicular to the ditch, three along the ditch bank, and a further one placed horizontally in the ditch along its bank. These arrays each consisted of a 4 m PVC rod containing 10 thermistors (S-THB, Onset, USA) located at 35 cm intervals from the bottom end. Ditch evaporation was measured using a floating evaporation pan, equipped with pressure sensors (Unik 5000, General Electric and 176PC, Honeywell, USA). Missing periods were filled using a fitted linear correction to calculated Penman evaporation values. Meteorological data were obtained from a meteorological station located on the south-eastern end of the field, consisting of a tipping bucket rain gage (ARG-100, Env. Systems, UK), solar radiation (SKS 1110 pyranometer, Skye Instr., UK), air humidity and temperature (HMP35, Vaisala, Finland), barometric pressure (VU Amsterdam, Netherlands), wind speed (A100R, Vector Instr., UK) and direction (W200P, Vector Instr., UK), and soil heat flux via thermocouple soil temperature measurements at 0.1 and 0.2 m depths. Crop condition and growth stage were inspected visually on a weekly basis. We measured soil hydraulic properties using both falling-head permeameter tests (Eijkelkamp, Netherlands) on core samples at different depths, and slug-tests (Beers, 1983) in existing piezometers. Continuous vertical electrical soundings (CVES; ABEM Terrameter SAS 4000, Sweden) with 0.5 m electrode spacings was performed on 29 March, 2012 and electromagnetic induction measurements were performed every 0.2 m in transects parallel to and perpendicular to the ditch on 11 February, 2014 (DUALEM 421, Dualem, Canada), to assess groundwater salinity distribution.

Measurement periods were from 30 May 2012 to 1 Dec 2012 and from 15 Apr 2013 to 1 Oct 2013. The measurement setup was partly dismantled in the intermediate period to allow field cultivation. Estimated measurement uncertainty of measured parameters and measurement devices is listed in Table 1. All ECs were converted to Total Dissolved Solids (TDS) using an EC-TDS relation derived specifically for the coastal region of the Netherlands (Stuyfzand, 2014), its applicability was checked using 26 available local chemical analyses (Appendix 1). To comprehensively investigate flow routes to the ditch, we subsequently: (1) established the hydrological response of the field to the prevailing meteorological conditions, (2) investigated groundwater salinity and the salinity dynamics in exfiltration to tile drains and the ditch, and the resulting surface water salinity response, (3) separated flow route contributions to exfiltration fluxes, (4) quantified the exfiltration flux response to groundwater level variations, and (5) investigated the hydrological and solute response of the field to both a wet and a dry period in more detail.

Table 1

2.3 Groundwater – surface water interaction

Unlike the exfiltration of groundwater via the tile drains, the direct flow of groundwater into and from the ditch could not be measured. We therefore deduced the transient surface water – groundwater (SW-GW) interaction in the ditch by simultaneously solving the water, salinity, and heat balance of the ditch (e.g., Assouline, 1993; Martínez-Alvarez et al., 2011; Xing et al., 2012). The simultaneous solution constrains uncertainty and allows for separation between the shallow and deeper flow paths to the ditch.

The water balance of the ditch can be written as:

$$q_{gw} = q_{out} - q_{in} - q_{pr} + q_e + \Delta V \text{ ,} \tag{1}$$

with q_{gw} denoting the SW-GW flux, q_{out} the measured ditch outflow, q_{in} the measured ditch intake flux, q_{pr} direct precipitation, q_e evaporation and ΔV the change in ditch volume (all in m^3, schematic overview in Figure 3). Note that Eq. 1 excludes the contribution of tile drains, as they are kept completely separate from the ditch. All parameters of Eq. 1 are measured quantities, except the SW-GW flux. Analogously, the salinity balance can be written as:

$$q_{gw}C_{gw} = q_{out}C_{out} - q_{in}C_{in} + \Delta S \text{ ,} \tag{2}$$

with C_i denoting the TDS (in g/L) of the various fluxes q_i, and ΔS the change in TDS storage (kg). Note that C_{gw} is the (unknown) flux-weighted mean TDS of exfiltrating groundwater, and that TDS of precipitation and evaporation are assumed zero (acceptable given the large TDS contrast between groundwater and precipitation). Finally, the heat balance, including terms for incoming radiation and sensible and latent heat loss but ignoring kinetic processes, reads (Anderson, 1952):

$$q_{gw}T_{\text{gw}} = q_{out}T_{out} - q_{in}T_{in} - q_{pr}T_{pr} + q_eT_e + \frac{1}{c_v}\left\{\rho_w\lambda\left(1+\beta\right)q_e - A\left(R_n - G\right)\right\} + \Delta H \text{ ,} \tag{3}$$

with T_i denoting the temperature (K) of the various fluxes q_i, c_v the volumetric heat capacity of water (MJ/m^{3}K), ρ_w water density (kg/m^3), λ the latent heat of vaporization (MJ/kg), β the Bowen ratio (-), A the ditch area (m^2), R_n the net radiation (MJ/m^2), G conduction through the ditch bottom (MJ/m^2), and ΔH the change in heat storage (m^{3}K). We calculated R_n from the available weather data using the standardized calculation procedure outlined in (Allen et al., 1998; Valiantzas, 2006), and β according to Bowen (1926). While generally neglected because of its small magnitude (Anderson, 1952;

Assouline, 1993), we included the conduction of heat through the ditch bottom *G* in the balance equation, as we expect the influence to be uncharacteristically large due to the large perimeter-volume-ratio. *G* becomes especially important when solving Eq. 3 on hourly time steps. Analogous to Eq. 2, T_{gw} is the (unknown) flux-weighted mean temperature of exfiltrating groundwater.

Denoting the known right hand sides of equations 1 – 3 as *W*, *S*, and *H*, the system of equations can be written in matrix form as:

$$\begin{bmatrix} 1 \\ C_{gw} \\ T_{gw} \end{bmatrix} \begin{bmatrix} q_{gw} \end{bmatrix} = \begin{bmatrix} W \\ S \\ H \end{bmatrix}; \qquad (4)$$

three linear equations with three unknowns: q_{gw}, C_{gw} and T_{gw}. Given these three unknowns, the system is well-determined, and the simultaneous solution has no purpose in constraining the uncertainty in q_{gw}. We therefore assumed the exfiltrating groundwater to be a conservative mixture of shallow (exfiltrating along the ditch edge) and deeper groundwater (exfiltrating in the centre of the ditch), of which we have measured both the EC (converted to TDS) and temperature (see coloured lines in Figure 3). By adding this extra information, Eq. 4 becomes the over-determined system:

$$\begin{bmatrix} 1 & 1 \\ C_{gw,s} & C_{gw,\mathrm{d}} \\ T_{gw,s} & T_{gw,d} \end{bmatrix} \begin{bmatrix} q_{gw,s} \\ q_{gw,d} \end{bmatrix} = \begin{bmatrix} W \\ S \\ H \end{bmatrix}, \tag{5}$$

with the subscripts *gw,s* and *gw,d* denoting shallow and deep groundwater flow paths respectively. So far, we only discussed the exfiltration situation. When infiltrating however, TDS and temperature of the infiltrating groundwater change to the TDS and temperature of the ditch, yielding the following nonlinear system of equations (note that the shallow and deep groundwater flux can no longer be distinguished in the infiltration situation):

$$\begin{gathered} \begin{bmatrix} 1 & 1 \\ C_{gw,s} & C_{gw,\mathrm{d}} \\ T_{gw,s} & T_{gw,d} \end{bmatrix} \begin{bmatrix} q_{gw,s} \\ q_{gw,d} \end{bmatrix} = \begin{bmatrix} W \\ S \\ H \end{bmatrix}, \text{ when } q_{gw} > 0 \\ \begin{bmatrix} 1 & 1 \\ C_{ditch} & C_{ditch} \\ T_{ditch} & T_{ditch} \end{bmatrix} \begin{bmatrix} q_{gw,s} \\ q_{gw,d} \end{bmatrix} = \begin{bmatrix} W \\ S \\ H \end{bmatrix}, \text{ when } q_{gw} < 0 \end{gathered} . \tag{6}$$

We solved this nonlinear system, with the added constraint that the sign of $q_{gw,s}$ should equal that of $q_{gw,d}$, using Sequential Least Squares Programming (Kraft, 1988) to minimize the sum of squares weighted by the inverse of right-hand-side variances. The additional constraint proved necessary to prevent fits with large opposite values of $q_{gw,s}$ and $q_{gw,d}$. In addition, we applied a Monte Carlo analysis (n=1000) to Eq. 6, randomly sampling Gaussian distributions around all measured parameters (using measurement variances reported in Table 1), to quantify the uncertainty in the calculated values of q_{gw}. Throughout the remainder of this paper, we refer to the (calculated) direct flow of groundwater into and from the ditch as ditch exfiltration and ditch infiltration respectively, and to the (measured) exfiltration of groundwater into the tile drains as drain exfiltration. The measured discharge of the ditch, the non-separated result of different flow routes, is referred to as ditch discharge.

3 Results

3.1 Water fluxes

The two measurement periods differed markedly in their meteorological conditions. The months of June to August 2012 were relatively wet (recurrence interval of the cumulative precipitation deficit 1.3 y, derived from a Gumbel distribution fitted to 50+ years of weather records of the nearby De Kooy meteorological station). The same period in 2013 was relatively dry (recurrence interval 14 y). These conditions were reflected in the measured hydrology of the field site (Figure 4, Table 2). Measured precipitation averaged 2.89 mm/d in 2012 (long-term average 2.45 mm/d for this period), while precipitation was limited to an average of 2.11 mm/d in 2013, including the wet period from 10 September 2013 onwards. Potential evapotranspiration, calculated according to the FAO Penman-Monteith method (Allen et al., 1998) and accounting for observed crop growth, amounted to 2.95 mm/d and 2.48 mm/d respectively. We assumed actual transpiration to match potential transpiration throughout the measurement period, due to the excellent water retention characteristics of the soil and used shallow soil moisture measurements to correct bare soil evaporation (Allen et al., 1998). Excess water is discharged from the field by exfiltration to both tile drains and ditches. Drain exfiltration was significantly higher than ditch exfiltration and averaged around 1.1 mm/d (2012) and 0.9 mm/d (2013). Ditch ex-/infiltration amounted to 0.1 mm/d of exfiltration in 2012, equal ditch infiltration and exfiltration fluxes of 0.2 mm/d added up to a net 0 mm/d in 2013 (note that all mm are areal averages over the entire field-plus-ditch area, unless stated otherwise). Closure of the water balance required between 1.2 mm/d (2012) and 0.9 mm/d (2013) of additional influx of water, mainly representing the influx of regional groundwater flow (Table 2).

<u>Figure 4</u>

<u>Table 2</u>

Measured groundwater levels reflect the varying meteorological conditions during the two measurement periods (Figure 4c). A succession of precipitation events throughout the 2012 measurement period resulted in rapidly changing groundwater levels, which remained above drain depth throughout the measurement period. Groundwater levels remained below the ground surface, peaking at 0.55 m BGS. Drier conditions in 2013 resulted in much less variation in groundwater levels between May and July 2013, after which groundwater levels dropped significantly below drainage depth and eventually ditch bottom, reaching a maximum depth of 1.65 m BGS. The dry period in 2013 prompted the farmer to irrigate the growing lettuce on two accounts (11 and 16 July 2013), leading to only small increases in soil moisture, and no noticeable effect on groundwater levels. Sprinkling water was obtained from the (not-instrumented) ditch bordering the field on its southern side. A large precipitation event on September 10 ended the long dry period and caused groundwater levels to quickly rise to a maximum of 0.7 m BGS.

The measurement and control setup aimed to keep the ditch water level at a level of 1.12 m BGS, just below drainage depth, and as constant as possible. However, the abundance of suspended fine-grained particulate and organic matter in the ditch caused filter clogging, which was a recurring issue before a redesign of the ditch filter on October 26, 2012. Large ditch water level variations between September 23 and October 26, 2012, were due to a rupture in the ditch culvert caused by mowing activities. Periods experiencing filter clogging, significant water level variations or power failures were discarded from further analyses.

We were able to separately measure both ditch discharge and intake and tile drain discharge in 15 minute increments for most of the measurement periods. All measurements were averaged to hourly periods for subsequent analyses. Tile drain discharge was on average 1.3 mm/d and varied between zero and 11.5 mm/d, showing a similar pattern to those of the observed groundwater levels. In 2012, drain discharge was sustained throughout the summer period. Drain discharge however ceased during the months of July and August 2013 after groundwater levels dropped below drainage depth. Drain discharge exhibited the characteristic tailing after a peak that is consistent with drainage theory (De Zeeuw and Hellinga, 1958; Kraijenhoff van de Leur, 1958). Ditch discharge was on average 0.2 mm/d and varied between -1.3 mm/d (intake) and 8.4 mm/d and was generally more gradual than tile drain discharge. An uncharacteristically large ditch discharge was recorded on September 10 2013, presumably due to a significant contribution of overland flow, caused by a large precipitation event (41 mm in 24 hours) following a prolonged dry period. Our measurement setup did not allow separating between overland flow and groundwater exfiltration.

<u>Figure 5</u>

Ditch floating evaporation pan measurements were only available for 2012. To extend the evaporation time series to 2013, we correlated measured open water evaporation to evaporation calculated using the standard Penman formula (Penman, 1948; Valiantzas, 2006) (Figure 5). Measured values correlated well with calculated values, but were consistently lower, and appeared to require a minimum amount of radiation ($E_{pan} = 0.48E_{Penman} – 0.73$, RMSE 0.62 mm/d). Calibration of the ‘wind function’ could not improve the calculation. Rather, deviations between measured and calculated values were predominantly related to an apparent overestimation of (net) incoming radiation.

We also operated a floating evaporation pan in the ditch on the southern end of the field. This ditch is both wider (3 m) and deeper (0.5 m) than the instrumented ditch. Penman evaporation estimates only slightly overestimated measured evaporation in this ditch ($E_{pan} = 0.84E_{Penman} – 0.32$, RMSE 0.93 mm/d). In all subsequent hourly analyses, we down-scaled daily evaporation values using hourly short-wave radiation measurements.

3.2 Groundwater and surface water salinity

Figure 6

Table 3

The main origin of exfiltrating solutes at the field site is the upward flow of brackish regional groundwater, exfiltrating in tile drains and ditches. Converted measurements of groundwater salinity showed an average TDS at 2 m BGS of 13.0 (± 1.4) g/L, whereas groundwater TDS at 1 m BGS is on average 0.43 (± 0.24) g/L. Average TDS of the tile drain discharge over the measurement periods was 3.3 g/L, while the average TDS of ditch discharge was 7.7 g/L over this period, signifying a preferential flow of higher-salinity groundwater to the ditch (Figure 6). Both drain and ditch salinity decreased during and increased between discharge events. Even though salinity of ditch discharge was significantly higher than tile drain discharge, salinity loads towards the surface water are dominated by tile drainage. Tile drains transported about three times more solutes than ditch exfiltration. The relative contribution of the ditch in the solute load increases between precipitation events however, reaching over 80% in prolonged dry periods. Table 3 lists the salinity balance of the field site, showing a necessarily large closure term reflecting the inability to measure the regional groundwater input to the salinity balance.

We determined the ditch surface water salinity that would have occurred without physical separation of flow routes by assuming complete mixing of the different flow paths entering the ditch with the resident ditch volume at each successive time step. In addition, we calculated the amount of flushing (assuming constant salinity of 0.7 g/L intake water) required to keep surface water TDS at 1.5 g/L , the local salinity norm for irrigating potatoes (Figure 6e). Unseparated ditch surface water salinity would have varied between about 3 to 7 g/L (excluding intake periods), both through salinity variations of drain and ditch exfiltration and through variation in the relative proportion of drain or ditch exfiltration in the ditch. Flushing demands vary significantly and may reach 25 mm/d (note that absolute amounts are conditional on the chosen salinity norm). The flushing demand was largely determined by the salt load entering the ditch and therefore reached peak values during discharge events, even though unflushed surface water salinity was then at its lowest. Calculated flushing demands were approximately equal to the sum of the other water balance components at the field site (Table 2).

Figure 7

Inversion results of CVES and DUALEM measurements (Figure 7), showed a clear pattern of brackish groundwater at very shallow depths (2 – 3 m BGS), overlain by fresher water. The CVES result has a much higher vertical resolution, and shows the upconing of brackish water towards the tile drains, located at 5 m intervals. An alternating pattern is visible in the upconing of brackish water to tile drains, likely related to the drains being alternately older and more recent, and could result from a lower drainage resistance of the newer tile drains (Velstra et al., 2013). The DUALEM system is a Frequency Domain EM (inductive coupling) system and, because of limited antenna orientations, offered a lower resolution in the vertical than CVES. DUALEM was, however, easier to operate on transects perpendicular to the field, crossing two ditches and a busy agricultural road. The low vertical resolution caused the inversion (EM4Soil) to calculate unrealistic increasing resistivities at greater depths. DUALEM results revealed the limited zone of influence (10 m) of the ditch on the salinity distribution beneath the agricultural field. Within this zone of influence, brackish water cones up towards the ditch. However, the results also indicate a small pocket of fresher water beneath the ditch bottom, which seems to indicate mixing with fresher water coming from the ditch sides. DUALEM results beneath the elevated road should be interpreted with caution, as the inversion was unable to adequately match the measured conductivities at lower depths. Still, results exclude the presence of a significant fresh water lens underneath the elevated road, possibly related to limited infiltration from the road surface. Low conductivities just below the road compared to the field resulted from lithological differences (sand bed below the road) and a lower moisture content.

3.3 Flow path separation

The simultaneous solution of the water-, salinity, and heat-balance of the ditch enabled the calculation of direct groundwater flow to and from the ditch (Figure 8, daily time step), and we assessed the associated uncertainty with a Monte Carlo analysis. Judging from the small uncertainty bands, the total groundwater exfiltration in the ditch could be well-discerned. Application of Eq. 6 further allowed the separation of ditch exfiltration in shallow and deep flow paths, based on the varying measured contrasts in both TDS and temperature, again with Monte Carlo-derived uncertainty ranges. The contrast in TDS was large and relatively constant at about 8 g/L, temperature contrast averaged only 0.2 °C and was more variable. In addition, assuming a fixed TDS for both regional groundwater flow and meteoric water, we straightforwardly separated tile drain discharge in meteoric and regional groundwater origins. Varying TDS between minimum and maximum measured values (12 – 17 g/L and 0 – 0.7 g/L for deep groundwater and meteoric water respectively) hardly affected the separation result, as demonstrated by the narrow uncertainty range surrounding the regional flow contribution to drain exfiltration. Note that the separations of ditch and tile drain exfiltration are not directly comparable, as the shallow flow path to the ditch in particular is itself a mixture of meteoric and regional groundwater.

Figure 8

Groundwater interaction with the ditch varied from a maximum infiltration rate of 1.4 mm/d, to a maximum exfiltration of 8.6 mm/d. These values were both slightly higher than the corresponding ditch intake / discharge, due to storage effects in the ditch and, to a lesser extent, to the contribution of precipitation and evaporation to the ditch water balance. The separation showed a consistently high contribution of deep regional groundwater to ditch exfiltration compared to drain exfiltration, in accordance with the measured salinity loads of the ditch. After the infiltration period in Aug 2013 however, the contribution of regional groundwater flow in ditch exfiltration was nearly zero. Groundwater that exfiltrated in the ditch during the subsequent precipitation event likely consisted primarily of water that infiltrated during the preceding period was attributed to the shallow flow path on account of its low salinity. The small peak in regional groundwater contribution just after the infiltration period probably resulted from water still stored in the collector reservoir from before the infiltration period. Excluding the peak possibly caused by overland flow, only 15 mm exfiltrated between Sep 10 and Oct 1, while a total of 29 mm infiltrated during the preceding period.

3.4 Hooghoudt drainage model

We analysed drain exfiltration (measured) and ditch exfiltration (calculated) versus measured head difference (Figure 9), which revealed a clear difference between the two.

While the relation was approximately linear for ditch exfiltration, drain exfiltration showed a much steeper and about exponential increase of exfiltration with increasing head difference. The steeper incline of drain exfiltration is a logical result of the lower resistance to flow to the tile drains. The exponential shape indicates a decrease in drainage resistance when groundwater levels rise. The lowering of the resistance to drainage when groundwater levels rise and the flow area increases is well-known in drainage theory, when the rise is significant relative to the total flow area (e.g., (Ernst, 1962; Hooghoudt, 1940)). This is represented by the second, quadratic term in the classic Hooghoudt equation (Hooghoudt, 1940):

$$q = \begin{cases} \dfrac{8k_2 D_{eff} m_0 + 4k_1 m_0^{\,2}}{L^2}, & \text{if } m_0 \geq 0 \\ \dfrac{8k_2 D_{eff} m_0 - 4k_1 m_0^{\,2}}{L^2}, & \text{if } m_0 < 0 \end{cases}, \qquad (7)$$

in which q is specific discharge (m/d), k_1 and k_2 are the hydraulic conductivity above and below the drainage level respectively (m/d), D_{eff} is the effective depth of flow (the total flow depth corrected to account for radial flow, calculated using (Moody, 1966)), m_0 is the groundwater level above drainage level at 0.5L, and L is the distance between drains (Hooghoudt, 1940). For the ditch, m_0 is the difference between the groundwater level at 0.5L and the ditch water level. Judging from fitting Eq. 7 to the data with a single hydraulic conductivity (12 cm/d), this phenomenon alone is not enough to explain the curvature apparent in Figure 9. A better approximation of the curvature in the drain data required a higher hydraulic conductivity above (k_1 = 50 cm/d) than below (k_2 = 1 cm/d) the drain depth (Figure 9).

Figure 9

The linear relation of ditch exfiltration indicates a negligible influence of head variations on the drainage resistance, pointing towards a significantly deeper flow system compared to the drains (first term in Eq. 7 >> second term). Flow towards the ditch could be well approximated applying Eq. 7 both for the southern (field) and northern side of the ditch, using a single hydraulic conductivity of 5 cm/d. Slug test-measured hydraulic conductivities ranged from 0.5 to 6 cm/d, whereas falling-head permeameter results of loamy-sand samples ranged from 2 to 6 cm/d (clayey top layer samples ranged from 0.001 to 0.3 cm/d (average 0.07 cm/d). Fitted hydraulic conductivities correspond well to measured values, especially for the linear domain. The slug tests were performed during a relatively dry period, when groundwater levels were only about 10 cm above drainage depth, so possibly could not capture a higher hydraulic conductivity at shallower depths. Note that drain exfiltration appeared to be maximized at about 0.7 mm/h, likely caused by the installed maximum pumping capacity (Figure 9). The ditch exfiltration values that exceed 0.7 mm/h, at a head difference of only 0.2 m, all occurred during the ditch discharge peak following the infiltration period of Aug 2013.

3.5 Individual events

3.5.1 Precipitation event

We took a closer look at the variation of drain and ditch exfiltration and their composition during a representative precipitation event that started October 29, 2012 (Figure 10). We therefore separated flow paths by applying Eq. 6 on an hourly instead of a daily time step. Uncertainty in calculated hourly ditch exfiltration proved to be relatively larger than uncertainty on a daily time step, predominantly due to the increased importance of (the uncertainty in) the storage terms in the hourly balance (Eq. 6). Nevertheless, the exfiltration process towards the ditch could be well identified.

Figure 10

Drain discharge lagged five hours behind the onset of precipitation, closely following the groundwater level response in the field, and again displayed the characteristic tailing-after-peak. The separation of drain exfiltration in shallow flow of local meteoric origin, and deep regional groundwater flow showed the preferential discharge of meteoric water during the discharge peak. TDS of drain exfiltration therefore decreased from 4.8 to 2.2 g/L. Still, the total salt flux exfiltrating via the tile drains increased, as the precipitation event also triggered a rise of the brackish deep flow component. Direct groundwater exfiltration to the ditch showed a similar pattern to drain exfiltration, albeit at a roughly seven times lower rate. Ditch exfiltration reacted faster and persisted longer compared to exfiltration to tile drains, corresponding with the observed pattern in groundwater head below and alongside (not shown) the ditch. The separation between shallow and deeper flow paths revealed a quick response of deeper groundwater, while the contribution of shallower flow paths lagged by about 12 hours. A similar pattern was observed for other events.

3.5.2 Infiltration event

Figure 11

Conditions were dry throughout July and August, 2013, causing a gradual decline in groundwater heads, to a maximum 5.6 m BSL (1.6 m BGS) (Figure 11). Exfiltration via the drains stopped on July 8 and exfiltration to the ditch switched to an infiltration situation quickly after. Infiltration was short-lived, as the ditch ran dry due to a mechanical failure in the intake system. This dry period lasted until July 31, when the intake possibility was restored. After an initial intake peak to restore the determined ditch water level, infiltration continued to follow the variation in head difference between surface and groundwater. Groundwater heads suddenly rose 8 and 7 cm below the ditch and in the field, respectively, within hours after intake was restored, showing no signs of a disconnect between ditch and groundwater. Groundwater heads subsequently continued their decline, but began to rise after 10 days of infiltration. Deviations from this pattern on August 14 and 15 are most likely only an artefact of combining hourly water level fluctuations with an only cumulatively known intake flux for that period (logger power failure). Preferential flow of the fluctuating ditch water to the then-submerged tile drains is the likely cause of the intermittent small tile drain exfiltration in August.

The lettuce crop was harvested on August 9 2013 and the field was tillaged on August 12. At about the same time, heads started to rise from 1.55 m BGS to a relatively stationary level of 1.2 m BGS that was reached on August 23. Groundwater heads both below the ditch, next to the ditch (not shown) and in the field showed a similar pattern. Whereas groundwater levels fell before harvesting as precipitation, upward regional groundwater flow and sideways infiltration from the ditch could not compensate for crop transpiration, groundwater levels recovered after harvesting. This is likely the result of a sharp decrease in evapotranspiration, as bare soil evaporation (corrected using shallow soil moisture measurements (Allen et al., 1998)) amounted to about 1 mm/d versus 3 mm/d if the crop had remained on the field.

Infiltration abruptly ended September 10, when 40 mm of precipitation resulted in a groundwater rise of 80 cm and both tile drain and ditch exfiltration were restored. Net infiltration over the preceding period totalled 27 mm, while only 0.4 mm (1.5 %) of ditch intake water was lost to evaporation. Note again that these values are areal averages over the entire field-plus-ditch area. Depending on the estimated storage difference of between 8 and 19 mm (16 cm head difference, assuming a specific yield between 0.05

and 0.12; literature range for the soil type considered (Wösten et al., 2013)), closure of the water balance during the infiltration period required between 0.5 to 1 mm/d of regional groundwater flow.

We observed diurnal patterns in the observed infiltration rates (Figure 11d), as well as in exfiltration rates during low-flow periods (not shown). The diurnal patterns were correlated to both ditch temperature variations, and diurnal patterns in groundwater heads. The amplitude of the infiltration variations, superimposed on the general trend of increasing infiltration rates, was 0.12 mm/d, or 10% of the concurrent infiltration rate. The concurrent 3 °C amplitude temperature variations could result in an 8 % variation in hydraulic conductivity (Constantz et al., 1994; Muskat, 1937). The amplitude of diurnal patterns in groundwater head, attributable to diurnal patterns in evapotranspiration in the field, was 2 cm, or 5% of the total head difference between surface water and groundwater.

4 Discussion

We instrumented an agricultural field to physically separate and measure the different flow paths contributing to the water and salinity balance of a headwater ditch, and specifically focused on agriculturally important summer periods. The on-going agricultural use of the field site proved challenging: our study suffered on several occasions from data loss due to filter clogging, power and mechanical failures.

Nevertheless, we were able to continuously measure tile drain outflow and both ditch outflow and intake for the majority of the meteorologically different 2012 and 2013 growing seasons. While direct measurement of groundwater exfiltration in the ditch was impossible, the simultaneous solution of the water, salinity and heat balance of the ditch enabled the quantification of ex- and infiltration of groundwater to and from the ditch. Although presumably an underestimation due to the inability to include epistemic, non-random errors in our analysis (Beven, 2006), Monte Carlo analysis indicated acceptable uncertainty in the exfiltration quantification. Upward flow of brackish regional groundwater at the field site resulted in a significant salinity contrast with infiltrating precipitation water. This contrast provided a unique opportunity to discern the different groundwater flow routes towards tile drains and the ditch and allowed for the mapping of the subsurface distribution of the two water types using geophysics.

We observed groundwater levels in the field to react within hours to precipitation events, even after prolonged dry periods, signifying only minor influence of the shallow unsaturated zone on the timing of discharge events. The response of tile drain and ditch exfiltration to groundwater levels could be satisfactorily characterized using conventional drainage theory (Hooghoudt, 1940), using hydraulic conductivities comparable to values measured in the field. Tile drains were fed by a shallow flow system. Drains responded nonlinearly to groundwater level variations, attributable to nonlinearity in drainage resistance and a possible increase in hydraulic conductivity upwards in the soil profile. Higher hydraulic conductivities near the ground surface have been frequently observed and linked to the presence of macropores in the soil (Beven and Germann, 2013, 1982; Tiktak et al., 2012). In contrast, groundwater flows to and from the ditch were linearly related to head differences, indicating a deep flow system and negligible influence of groundwater level variations on drainage resistance. Alternatively, anisotropy could also be a factor in explaining the observed differences in apparent hydraulic conductivity between the shallow, strongly radial flow to tile drains and the deeper flow paths to the ditch (Smedema et al., 1985). Our results showed no evidence for differences in resistance between exfiltration and infiltration that have been observed in other settings and attributed to clogging processes (Blaschke et al., 2003; Cox et al., 2007; Doppler et al., 2007). Ditch in- and exfiltration rates showed diurnal patterns that likely resulted from both the temperature-dependence of hydraulic conductivity (Constantz et al., 1994; Muskat, 1937) and evapotranspiration-induced diurnal head variations.

Geophysical measurements disclosed the presence of brackish groundwater, originating from regional groundwater flow, within two m BGS. Brackish groundwater showed previously reported (De Louw et al., 2013, 2011a; Velstra et al., 2011) upconing patterns towards the tile drains, while measurements indicated the exfiltration of brackish groundwater along the entire wet perimeter of the ditch. Consequently, salinity of ditch exfiltration was significantly higher than tile drain exfiltration (TDS of 11 and 3.6 g/L respectively, excluding the post-infiltration period, when the exfiltration to the ditch consisted of previously infiltrated intake water). Salts were transported to surface water in a complex, time-varying pattern. While tile drainage was the dominant source of salt input in to surface water during the study period (80%, Table 3), the composition of salt origin was highly variable. Tile drains dominated the salt load during discharge events, but 80% of the ditch water composition during drier periods originated from ditch exfiltration (Figure 6). During discharge events, tile drain salinity decreased by about 50%, pointing to a larger proportion of discharge originating from shallow flow paths delivering fresh water to the tile drains. This pattern corresponds to previous observations in similar settings (De Louw et al., 2013; Velstra et al., 2011). Ditch exfiltration salinity on the other hand first increased, then decreased over the course of discharge events, concurrent with the observed responses of the shallow and deep flow paths to the ditch. While the observed pattern in tile drain salinity has been attributed to preferential flow of meteoric water via macropores (De Louw et al., 2013; Velstra et al., 2011), such a mechanism would not explain the observed initial rise in ditch exfiltration salinity. We conceptualize the different timings of water with shallow and deep signatures to arise from the difference between pressure wave celerity and water velocity. Pressure is quickly propagated through the subsurface and flow directions change accordingly when groundwater levels rise. However, the salinity distribution lags behind, as it requires the actual flow of groundwater to change the salinity distribution. This difference results in the preferential exfiltration of groundwater with a deep flow path signature, as this groundwater type is initially also exfiltrated by shallow flow paths (Figure 12b, shallow flow paths intersecting lagging saline deep groundwater type). Water with a shallow flow path signature only reaches the ditch when the dynamic equilibrium between flow direction and salinity distribution is restored, thereby decreasing exfiltration salinity (Figure 12c). Quantifying the timing of deep and shallow flow path response may therefore prove useful in inferring subsurface properties (e.g., effective porosity), but was outside the scope of this research.

<u>Figure 12</u>

Standard water management practice of polders in the Netherlands supports their mainly agricultural use and entails diverting fresh river water to supplement summer precipitation deficits and dilute surface water salinity levels using a more or less constant flushing regime to enable sprinkling irrigation. Surface water demands of the field site averaged over the dry growing season of 2013 were largest for flushing (2.4 mm/d; calculated value), then sprinkling irrigation (0.4 mm/d), and finally groundwater infiltration (0.2 mm/d), while open water evaporation was negligible. Combined demands to enable sprinkling irrigation were therefore over six times the irrigation amount in the 2013 growing season. Despite the large upward flow of regional groundwater in the studied polder, we found ditch infiltration to constitute a significant loss of diverted river water, amounting to a maximum of 1.5 mm/d over the catchment area (188 mm/d per ditch length unit). Low evaporation from the ditch resulted in evaporation accounting for only 1.5% of intake loss during the infiltration period (the remainder lost to infiltration). Evaporation from the instrumented ditch was, however, poorly estimated using the routinely applied Penman formula, which overestimated ditch evaporation by a factor of two. Evaporation measurements from a different ditch revealed large differences in evaporation rates between ditches; further study is necessary to unravel the specific processes steering evaporation from small ditches and better predict ditch evaporation. Calculated flushing demands varied widely over time, controlled by the salt load entering the ditch; demands were high during wet periods and low during dry periods. As sprinkling irrigation is only applied during dry periods, this result could imply significant water savings when flushing is either operationally controlled, dependent on salinity levels and sprinkling needs, or set to a constant flux calibrated to accommodate only dry periods.

We did not specifically address density effects in our analyses, other than correcting head measurements. However, Simmons (2005) argued the importance of including density effects when studying groundwater flow, even when only small concentration gradients exist, by equating a typical head gradient of 10^{-3} to the density effect caused by a density difference of 1 kg/m^3 (5% seawater). In an agricultural setting similar to our field site, with head gradients in the order of 10^{-1} m, (De Louw et al., 2011a) found negligible influence of variable-density flow. Head gradients in the Schermer polder field site are also in the order of 10^{-1} m, while density differences are maximum 8 kg/m^3 (Post, 2012), suggesting only minor influence of density effects on groundwater flow. Still, density could be an important factor in drier periods, when head gradients are smaller. For instance, density could influence the infiltration rate induced by a head gradient of

0.025 (August 23 – September 5, 2013) by over 30 %. We aim to further address the influence of density differences in further work.

5 Conclusion

This study presents results of high frequency measurements of groundwater – surface water interaction in an instrumented agricultural field in a deep polder in the coastal region of the Netherlands. Simultaneous measurements of discharge, electrical conductivity and temperature allowed the separation and investigation of flow paths transporting water and salts to surface water, and disclosed complex and time-varying patterns of tile drain and ditch exfiltrationDespite their lower salinity, tile drains transported the majority of salts to surface water. Salinity of exfiltrating drain and ditch water appeared governed by the interplay between the fast-responding pressure distribution in the subsurface that determined groundwater flow paths (wave celerity), and the slow-responding groundwater salinity distribution (water velocity).

This study was motivated by the need for improved water management strategies for Dutch polders, to cope with increasing water scarcity and increasing exfiltration of brackish regional groundwater. This study has provided important insight in the processes determining surface water salinity, diverted river water demand and the influence of water management (ditch water level, drain design and flushing rates). Our findings suggest possible direct savings in flushing demands, and open the way to establish improved hydrological polder models, useful for both operational management of fresh water resources and the evaluation of future water management strategies.

6 Acknowledgements

This research was carried out within the Dutch Knowledge for Climate program. Field measurements were partly supported by Stichting SKB, we thank Jouke Velstra for the cooperation and interesting discussions. We thank Jacob Oosterwijk, Kyra Hu-a-ng, Sonia Borja-Quintero, Pieter Winters, Pieter Pauw, Frans Backer, and Harry Massop for assisting with field measurements. This paper benefited from discussions with Frans van Geer, Jan van Bakel, Aris Lourens, Pieter Pauw, Perry de Louw and Gualbert Oude Essink. We are most grateful to Ted Vaalburg for allowing his field and ditch to be the subject of this study. We thank three anonymous reviewers for improving this manuscript.

Appendix A: EC - Total Dissolved Solids (TDS) Conversion

The concentration of total dissolved solids (TDS) in water is accurately calculated by summing up all individual components (excluding gases):

$$\begin{aligned}\mathrm{TDS} = {} & \sum \text{major cations} + \sum \text{major anions} + 10^{-(\mathrm{pH}-3)} + \\ & \sum \text{trace elements (excl. gases)} + \mathrm{SiO_2} + 2.5\mathrm{DOC}\end{aligned}, \qquad \text{(A.1)}$$

with major cations Na^+, K^+, Ca^{2+}, Mg^{2+}, Fe^{2+}, Mn^{2+} and Al^{3+}, and major anions Cl^-, SO_4^{2-}, HCO_3^-, CO_3^{2-}, NO_3^-, PO_4^{3-} (all in mg/L). The factor 2.5 in Eq. 8 is needed to convert organic carbon to organic material simplified as CH_2O.

Alternatively, when ion concentrations are not available, TDS can be approximated by an often linear relation with measured Electrical Conductivity (EC). Such relations are necessarily site-specific, as different ionic ratios influence the TDS – EC relation.

Stuyfzand (2014) reports a TDS – EC relation derived for the coastal region of the Netherlands, suitable for TDS concentrations ranging from dilute rainwater to brine. The relation is linear for low EC_{20} values, and switches to a higher-order polynomial above an EC_{20} of 200 μS/cm:

$$\mathrm{TDS} = \begin{cases} 0.698\mathrm{EC}_{20}, & \text{if } \mathrm{EC}_{20} \leq 200 \\ 4.059\cdot10^{-21}\mathrm{EC}_{20}^{\;5} - 1.449\cdot10^{-15}\mathrm{EC}_{20}^{\;4} + 1.832\cdot10^{-10}\mathrm{EC}_{20}^{\;3} - & \\ \quad 6.974\cdot10^{-6}\mathrm{EC}_{20}^{\;2} + 0.8365\mathrm{EC}_{20} - 0.5, & \text{if } \mathrm{EC}_{20} > 200 \end{cases}, \quad (\mathrm{A.2})$$

with TDS in mg/L, and EC_{20} in μS/cm. Average error of Eq. A.2 was found to be 13.1% (Stuyfzand, 2014).

We established the applicability of the above relation for local conditions at the study site by comparing TDS according to Eqs. A.1 and A.2 for 26 local samples of shallow groundwater at different depths. Laboratory results of these samples were checked according to guidelines outlined by Stuyfzand (2014). Average error of local samples was found to be 9.9%, well within the average error of the original dataset. Figure A1 shows the local samples plotted alongside the original dataset used for the derivation of Eq. A.2.

Figure A.1

References

Aerts, J., Major, D.C., Bowman, M.J., Dircke, P., Aris Marfai, M., others, 2009. Connecting delta cities: coastal cities, flood risk management and adaptation to climate change. VU University Press, Amsterdam, Netherlands.

Allen, R., Pereira, L., Raes, D., Smith, M., 1998. Crop evapotranspiration-Guidelines for computing crop water requirements-FAO Irrigation and drainage paper 56, FAO, Rome. Rome, Italy.

Anderson, R., 1952. Energy Budget Studies, in: Harbeck Jr, G., Dennis, P., Kennon, F., Anderson, R. (Eds.), Water Loss Investigations, Vol.1, Lake Hefner Studies. US Geological Survey Circular 229, Washington, DC.

Assouline, S., 1993. Estimation of lake hydrologic budget terms using the simultaneous solution of water, heat, and salt balances and a Kalman Filtering Approach: Application to Lake Kinneret. Water Resour. Res. 29, 3041–3048. doi:10.1029/93WR01181

Barfuss, S., Johnson, M., Neilsen, M., 2011. Accuracy of In-Service Water Meters at Low and High Flow Rates.

Basu, N.B., Destouni, G., Jawitz, J.W., Thompson, S.E., Loukinova, N. V., Darracq, A., Zanardo, S., Yaeger, M., Sivapalan, M., Rinaldo, A., Rao, P.S.C., 2010. Nutrient loads exported from managed catchments reveal emergent biogeochemical stationarity. Geophys. Res. Lett. 37, n/a–n/a. doi:10.1029/2010GL045168

Beers, W. Van, 1983. The Auger Hole Method - A field measurement of the hydraulic conductivity of soil below the water table.

Beven, K.J., Germann, P., 1982. Macropores and water flow in soils. Water Resour. Res. 18, 1311–1325.

Beven, K.J., Germann, P., 2013. Macropores and water flow in soils revisited. Water Resour. Res. 49, 3071–3092. doi:10.1002/wrcr.20156

Blaschke, A., Steiner, K., Schmalfuss, R., Gutknecht, D., Sengschmitt, D., 2003. Clogging processes in hyporheic interstices of an impounded river, the Danube at Vienna, Austria. Int. Rev. Hydrobiol. 88, 397–413.

Bosman, H., 1993. A method for discriminating between evaporation and seepage losses from open water canals. Water SA 19, 171–175.

Bowen, I., 1926. The ratio of heat losses by conduction and by evaporation from any water surface. Phys. Rev. 721.

Campbell Sci, 2011. CS616 and CS625 Water Content Reflectometers. Logan, USA.

Constantz, J., Thomas, C., Zellweger, G.W., 1994. Influence of diurnal variations in stream temperature on streamflow loss and groundwater recharge. Water Resour. Res. 30, 3253–3264.

Cox, M.H., Su, G.W., Constantz, J., 2007. Heat, chloride, and specific conductance as ground water tracers near streams. Ground Water 45, 187–95. doi:10.1111/j.1745-6584.2006.00276.x

Custodio, E., Bruggeman, G.A., 1987. Groundwater problems in coastal areas., Studies an. ed, Studies and Reports in Hydrology (UNESCO), Studies and Reports in Hydrology (UNESCO). UNESCO, Paris.

De Louw, P.G.B., Eeman, S., Oude Essink, G.H.P., Vermue, E., Post, V.E.A., 2013. Rainwater lens dynamics and mixing between infiltrating rainwater and upward saline groundwater seepage beneath a tile-drained agricultural field. J. Hydrol. 501, 133–145. doi:10.1016/j.jhydrol.2013.07.026

De Louw, P.G.B., Eeman, S., Siemon, B., Voortman, B.R., Gunnink, J.L., van Baaren, E.S., Oude Essink, G.H.P., 2011a. Shallow rainwater lenses in deltaic areas with saline seepage. Hydrol. Earth Syst. Sci. 15, 3659–3678. doi:10.5194/hess-15-3659-2011

De Louw, P.G.B., Oude Essink, G.H.P., Stuyfzand, P.J., Van der Zee, S.E.A.T.M., 2010. Upward groundwater flow in boils as the dominant mechanism of salinization in deep polders, The Netherlands. J. Hydrol. 394, 494–506. doi:10.1016/j.jhydrol.2010.10.009

De Louw, P.G.B., Van der Velde, Y., Van der Zee, S., 2011b. Quantifying water and salt fluxes in a lowland polder catchment dominated by boil seepage: a probabilistic end-member mixing approach. Hydrol. Earth Syst. Sci. 15, 2101–2117. doi:10.5194/hess-15-2101-2011

De Zeeuw, J.W., Hellinga, F., 1958. Neerslag en afvoer. Landbouwkd. Tijdschr. 70, 405–422.

Delsman, J.R., Hu-a-ng, K.R.M., Vos, P.C., De Louw, P.G.B., Oude Essink, G.H.P., Stuyfzand, P.J., Bierkens, M.F.P., 2014. Paleo-modeling of coastal saltwater intrusion during the Holocene: an application to the Netherlands. Hydrol. Earth Syst. Sci. 18, 3891–3905. doi:10.5194/hess-18-3891-2014

Delsman, J.R., Oude Essink, G.H.P., Beven, K.J., Stuyfzand, P.J., 2013. Uncertainty estimation of end-member mixing using generalized likelihood uncertainty estimation (GLUE), applied in a lowland catchment. Water Resour. Res. 49, 4792–4806. doi:10.1002/wrcr.20341

Delta Programme Commissioner, 2013. Delta Programme 2014 - Working on the delta, Promising solutions for tasking and ambitions. The Hague, Netherlands.

Doppler, T., Franssen, H.-J.H., Kaiser, H.-P., Kuhlman, U., Stauffer, F., 2007. Field evidence of a dynamic leakage coefficient for modelling river–aquifer interactions. J. Hydrol. 347, 177–187. doi:10.1016/j.jhydrol.2007.09.017

Eertwegh, G. Van den, Meinardi, C., 1999. Water-en nutrientenhuishouding van het stroomgebied van de Hupselse beek. Wageningen, Netherlands.

EML, 2009. ARG100 – Rainfall Intensity Adjustments. North Shields, UK.

Ernst, L., 1962. Grondwaterstromingen in de verzadigde zone en hun berekening bij aanwezigheid van horizontale evenwijdige open leidingen (PhD thesis). Centrum voor Landbouwpublikaties en Landbouwdocumentatie.

Forzieri, G., Feyen, L., Rojas, R., Flörke, M., Wimmer, F., Bianchi, a., 2014. Ensemble projections of future streamflow droughts in Europe. Hydrol. Earth Syst. Sci. 18, 85–108. doi:10.5194/hess-18-85-2014

General Electric, 2012. UNIK 5000 Pressure Sensing Platform.

Griffioen, J., Vermooten, S., Janssen, G., 2013. Geochemical and palaeohydrological controls on the composition of shallow groundwater in the Netherlands. Appl. Geochemistry 39, 129–149. doi:10.1016/j.apgeochem.2013.10.005

Honeywell, 2012. 176PC07HD2 Product specifications. Minneapolis, USA.

Hooghoudt, S.B., 1940. Algemeene beschouwing van het probleem van de detailontwatering en de infiltratie door middel van parallel loopende drains, greppels, slooten en kanalen. Bijdr. tot kennis van eenige natuurkundige grootheden van den grond.

I.C.W., 1982. Quantity and quality of ground- and surface water in Noord-Holland north of the IJ [in Dutch].

Kahlown, M.A., Kemper, W.D., 2004. Seepage losses as affected by condition and composition of channel banks. Agric. Water Manag. 65, 145–153. doi:10.1016/j.agwat.2003.07.006

Kennedy, C.D., Bataille, C., Liu, Z., Ale, S., VanDeVelde, J., Roswell, C.R., Bowling, L.C., Bowen, G.J., 2012. Dynamics of nitrate and chloride during storm events in agricultural catchments with different subsurface drainage intensity (Indiana, USA). J. Hydrol. 466-467, 1–10. doi:10.1016/j.jhydrol.2012.05.002

Kraft, D., 1988. A software package for sequential quadratic programming. DFVLR Obersfaffeuhofen, Germany, Koeln, Germany.

Kraijenhoff van de Leur, D.A., 1958. A study of non-steady groundwater flow with special reference to a reservoir-coefficient. Ing. 70, 87–94.

Makkink, G.F., 1957. Testing the Penman formula by means of lysimeters. J. Inst. Water Eng. 11, 277–288.

Martínez-Alvarez, V., Gallego-Elvira, B., Maestre-Valero, J.F., Tanguy, M., 2011. Simultaneous solution for water, heat and salt balances in a Mediterranean coastal lagoon (Mar Menor, Spain). Estuar. Coast. Shelf Sci. 91, 250–261. doi:10.1016/j.ecss.2010.10.030

Montanari, A., Young, G., Savenije, H.H.G., Hughes, D., Wagener, T., Ren, L.L., Koutsoyiannis, D., Cudennec, C., Toth, E., Grimaldi, S., Blöschl, G., Sivapalan, M., Beven, K., Gupta, H., Hipsey, M., Schaefli, B., Arheimer, B., Boegh, E., Schymanski, S.J., Di Baldassarre, G., Yu, B., Hubert, P., Huang, Y., Schumann, A., Post, D. a., Srinivasan, V., Harman, C., Thompson, S., Rogger, M., Viglione, A., McMillan, H., Characklis, G., Pang, Z., Belyaev, V., 2013. “Panta Rhei—Everything Flows”: Change in hydrology and society—The IAHS Scientific Decade 2013–2022. Hydrol. Sci. J. 58, 1256–1275. doi:10.1080/02626667.2013.809088

Moody, W.T., 1966. Nonlinear differential equation of drain spacing. J. Irrig. Drain. Div. Amer. Soc. Civ. Eng 92, 1–9.

Muskat, M., 1937. The flow of homogeneous fluids through porous media. McGraw-Hill, New York.

Onset, 2013. 12-Bit Temperature Smart Sensor (Part # S-TMB-M0XX).

Oosterwijk, J., 2009. Waterbalansstudie Schermer [in Dutch]. Gouda, Netherlands.

Penman, H., 1948. Natural evaporation from open water, bare soil and grass. Proc. R. Soc. Lond. A. Math. Phys. Sci. 193, 120–145.

Post, V.E.A., 2012. Electrical Conductivity as a Proxy for Groundwater Density in Coastal Aquifers. Ground Water 50, 785–92. doi:10.1111/j.1745-6584.2011.00903.x

Post, V.E.A., Kooi, H., Simmons, C.T., 2007. Using hydraulic head measurements in variable-density ground water flow analyses. Ground Water 45, 664–71. doi:10.1111/j.1745-6584.2007.00339.x

Post, V.E.A., Plicht, H., Meijer, H., 2003. The origin of brackish and saline groundwater in the coastal area of the Netherlands. Netherlands J. Geosci. / Geol. en Mijnb. 82, 133–147.

Rozemeijer, J.C., Broers, H.P., 2007. The groundwater contribution to surface water contamination in a region with intensive agricultural land use (Noord-Brabant, The Netherlands). Environ. Pollut. 148, 695–706. doi:10.1016/j.envpol.2007.01.028

Rozemeijer, J.C., Siderius, C., Verheul, M., Pomarius, H., 2012. Tracing the spatial propagation of river inlet water into an agricultural polder area using anthropogenic gadolinium. Hydrol. Earth Syst. Sci. 16, 2405–2415. doi:10.5194/hess-16-2405-2012

Rozemeijer, J.C., Van der Velde, Y., Van Geer, F.C., Bierkens, M.F.P., Broers, H.P., 2010. Direct measurements of the tile drain and groundwater flow route contributions to surface water contamination: From field-scale concentration patterns in groundwater to catchment-scale surface water quality. Environ. Pollut. 158, 3571–9. doi:10.1016/j.envpol.2010.08.014

Schlumberger, 2010. Diver product manual.

Schultz, B., 1992. De waterbeheersing van droogmakerijen (PhD thesis). Faculty of Civil Engineering and Geosciences, Delft University of Technology.

Simmons, C.T., 2005. Variable density groundwater flow: From current challenges to future possibilities. Hydrogeol. J. 13, 116–119. doi:10.1007/s10040-004-0408-3

Skye Instr., 2009. Solar Radiation System for Photo Voltaics. Llandrindod Wells, UK.

Smedema, L., Poelman, A., Haan, W. De, 1985. Use of the Hooghoudt formula for drain spacing calculations in homogeneous-anisotropic soils. Agric. water Manag. 10, 283–291.

Sophocleous, M., 2002. Interactions between groundwater and surface water: the state of the science. Hydrogeol. J. 10, 52–67. doi:10.1007/s10040-001-0170-8

Stuyfzand, P.J., 1993. Hydrochemistry and hydrology of the coastal dune area of the Western Netherlands (PhD thesis). Faculty of Earth Sciences, VU University Amsterdam.

Stuyfzand, P.J., 2014. Hydrogeochemcal (HGC 2.1), for storage, management, control, correction and interpretation of water quality data in Excel spread sheet, KWR-report BTO.2012.244(s)), update of 2012 report.

Tiemeyer, B., Kahle, P., Lennartz, B., 2006. Nutrient losses from artificially drained catchments in North-Eastern Germany at different scales. Agric. Water Manag. 85, 47–57. doi:10.1016/j.agwat.2006.03.016

Tiktak, A., Hendriks, R.F.A., Boesten, J.J.T.I., Van der Linden, A.M.A., 2012. A spatially distributed model of pesticide movement in Dutch macroporous soils. J. Hydrol. 470-471, 316–327. doi:10.1016/j.jhydrol.2012.09.025

Vaisala, 1998. HMI38 Humidity data processor and HMP35/36/37E probes - Operating manual.

Valiantzas, J.D., 2006. Simplified versions for the Penman evaporation equation using routine weather data. J. Hydrol. 331, 690–702. doi:10.1016/j.jhydrol.2006.06.012

Van den Eertwegh, G.A.P.H., 2002. Travel times of drainage water and nutrient loads to surface water. Wageningen University.

Van der Velde, Y., De Rooij, G.H., Rozemeijer, J.C., Van Geer, F.C., Broers, H.P., 2010a. Nitrate response of a lowland catchment: On the relation between stream concentration and travel time distribution dynamics. Water Resour. Res. 46, 1–17. doi:10.1029/2010WR009105

Van der Velde, Y., Rozemeijer, J.C., De Rooij, G.H., Van Geer, F.C., Broers, H.P., 2010b. Field-Scale Measurements for Separation of Catchment Discharge into Flow Route Contributions. Vadose Zo. J. 9, 25. doi:10.2136/vzj2008.0141

Van Rees Vellinga, E., Toussaint, C., Wit, K., 1981. Water quality and hydrology in a coastal region of the Netherlands. J. Hydrol. 50, 105–127.

Velstra, J., Groen, K., De Jong, K., 2011. Observations of Salinity Patterns in Shallow Groundwater and Drainage Water From Agricultural Land in the Northern Part of the Netherlands. Irrig. Drain. 60, 51–58. doi:10.1002/ird.675

Velstra, J., Oosterwijk, J., Oord, A., 2013. Pilot Ecoboeren, Schermer-Zuid, Noord-Holland [in Dutch]. Gouda, Netherlands.

Von Asmuth, J., 2010. Over de kwaliteit , frequentie en validatie van druksensorreeksen [On the Quality, Frequency and Validation of Pressure Sensor Time Series, in Dutch], Water. Nieuwegein, Netherlands.

Weerts, H.J.T., Westerhoff, W.E., Cleveringa, P., Bierkens, M.F.P., Veldkamp, J.G., Rijsdijk, K.F., 2005. Quaternary geological mapping of the lowlands of The Netherlands, a 21st century perspective. Quat. Int. 133-134, 159–178. doi:10.1016/j.quaint.2004.10.011

Wösten, H., De Vries, F., Hoogland, T., Massop, H., Veldhuizen, A.A., Vroon, H., Wesseling, J., Heijkers, J., Bolman, A., 2013. BOFEK2012, de nieuwe, bodemfysische schematisatie van Nederland [BOFEK2012; the new soil physical schematization of the Netherlands, in Dutch]. Wageningen.

Xing, Z., Fong, D. a., Tan, K.M., Lo, E.Y.-M., Monismith, S.G., 2012. Water and heat budgets of a shallow tropical reservoir. Water Resour. Res. 48, W06532. doi:10.1029/2011WR011314

Table 1 Estimated measurement uncertainty for measured parameters

Parameter	*Device*	*Estimated uncertainty* [a]	*Source*
Groundwater head	Schlumberger Diver	± 0.002 m	(Schlumberger, 2010)
Ditch water level	Schlumberger Diver	± 0.02 m [b]	(Von Asmuth, 2010)
Ditch water level	GE Unik 5000	± 0.002 m	(General Electric, 2012)
Discharge	Itron propeller flow meter	± 1.5% [c]	(Barfuss et al., 2011)
Evap pan water level	GE Unik 5000	± .002 m	(General Electric, 2012)
Evap pan water level	Honeywell 176PC	± .002 m	(Honeywell, 2012)
Groundwater EC25	Schlumberger CTD-Diver	± 1.0% [c]	(Schlumberger, 2010)
Gw temperature	Onset S-THB	± 0.2 °C	(Onset, 2013)
Soil moisture	Campbell Sci CS616	± 2.5%VWC	(Campbell Sci, 2011)
Precipitation	EML ARG-100	± 0.1 mm	(EML, 2009)
Solar radiation	Skye Instr. SKS 1110	± 5.0% [c]	(Skye Instr., 2009)
Air humidity	Vaisala HMP-35	± 2.0% [c]	(Vaisala, 1998)
Air temperature	Vaisala HMP-35	± 0.1 °C	(Vaisala, 1998)
Barometric pressure	VU Amsterdam	± 1 hPa	VU, pers. comm.
Hydraulic conductivity	Eijkelkamp permeameter	± 130% [c]	*Measurement repetition*
Hydraulic conductivity	Slug tests	± 35% [c]	*Measurement repetition*

[a] Uncertainty is reported as 2 * standard deviation, unless stated otherwise

[b] Higher than groundwater head due to larger temperature differences

[c] 2 * relative standard deviation

Table 2 Water balance field site

Parameter	*June – Sept 2012*[a]		*June – Sept 2013*	
	mm/d	%	mm/d	%
Precipitation	2.89	70.4%	2.11	57.9%
Sprinkler irrigation[b]	0.00	0.0%	0.41	11.1%
Ditch infiltration[c]	0.01	0.2%	0.19	5.3%
Total in	2.90	70.5%	2.71	74.3%
Evapotranspiration	2.95	71.7%	2.48	67.9%
Tile drain exfiltration	1.06	25.7%	0.94	25.7%
- shallow flow path[c]	0.80	19.5%	0.78	21.5%
- deep flow path[c]	0.26	6.2%	0.15	4.2%
Ditch exfiltration[c]	0.09	2.2%	0.19	5.2%
- shallow flow path[c]	0.05	1.1%	0.16	4.4%
- deep flow path[c]	0.04	1.0%	0.03	0.8%
Storage change	0.01	0.3%	0.04	1.2%
Total out	4.11	100.0%	3.65	100.0%
Closure	1.21	29.5%	0.94	25.7%
(Flushing demand)[c,d]	4.93	117.5%	2.36	64.5%

[a] Limited to the period 15 June – 23 September due to system malfunction

[b] Estimated irrigation amount of 25 mm per event

[c] Based on calculation rather than direct measurement

[d] Based on norm TDS of 1.5 g/L and intake water TDS of 0.7 g/L

ACCEPTED MANUSCRIPT

Table 3 TDS balance field site

Parameter	*June – Sept 2012*[a]		*June – Sept 2013*	
	kg/d	%	kg/d	%
Precipitation[b]	0.53	2.4%	0.39	2.7%
Fertilizer application[c]	0.24	1.1%	0.24	1.6%
Sprinkler irrigation[d]	0.00	0.0%	1.31	9.0%
Ditch infiltration[e]	0.40	1.8%	0.86	5.9%
Total in	1.17	5.3%	2.79	19.1%
Evapotranspiration[f]	0.25	1.1%	0.20	1.4%
Tile drain exfiltration	17.50	79.2%	11.89	81.5%
- shallow flow path[e]	1.94	8.8%	1.77	12.1%
- deep flow path[e]	15.56	70.4%	10.12	69.4%
Ditch exfiltration[e]	4.35	19.7%	2.49	17.1%
- shallow flow path[e]	1.11	5.0%	0.64	4.4%
- deep flow path[e]	3.23	14.6%	1.85	12.7%
Storage change	?	?	?	?
Total out	22.09	100.0%	14.58	100.0%
Closure	20.92	94.7%	11.79	80.9%

[a] Limited to the period 15 June – 23 September due to system malfunction

[b] Bulk TDS precipitation 48 mg/L (Stuyfzand, 1993)

[c] Estimated at 100 kg/ha/j Cl (Eertwegh and Meinardi, 1999)

[d] Estimated irrigation amount of 25 mm per event, TDS measured

[e] Based on calculation rather than direct measurement

[f] From estimated plant uptake concentration of 10 mg/L Cl (Van der Velde et al., 2010a)

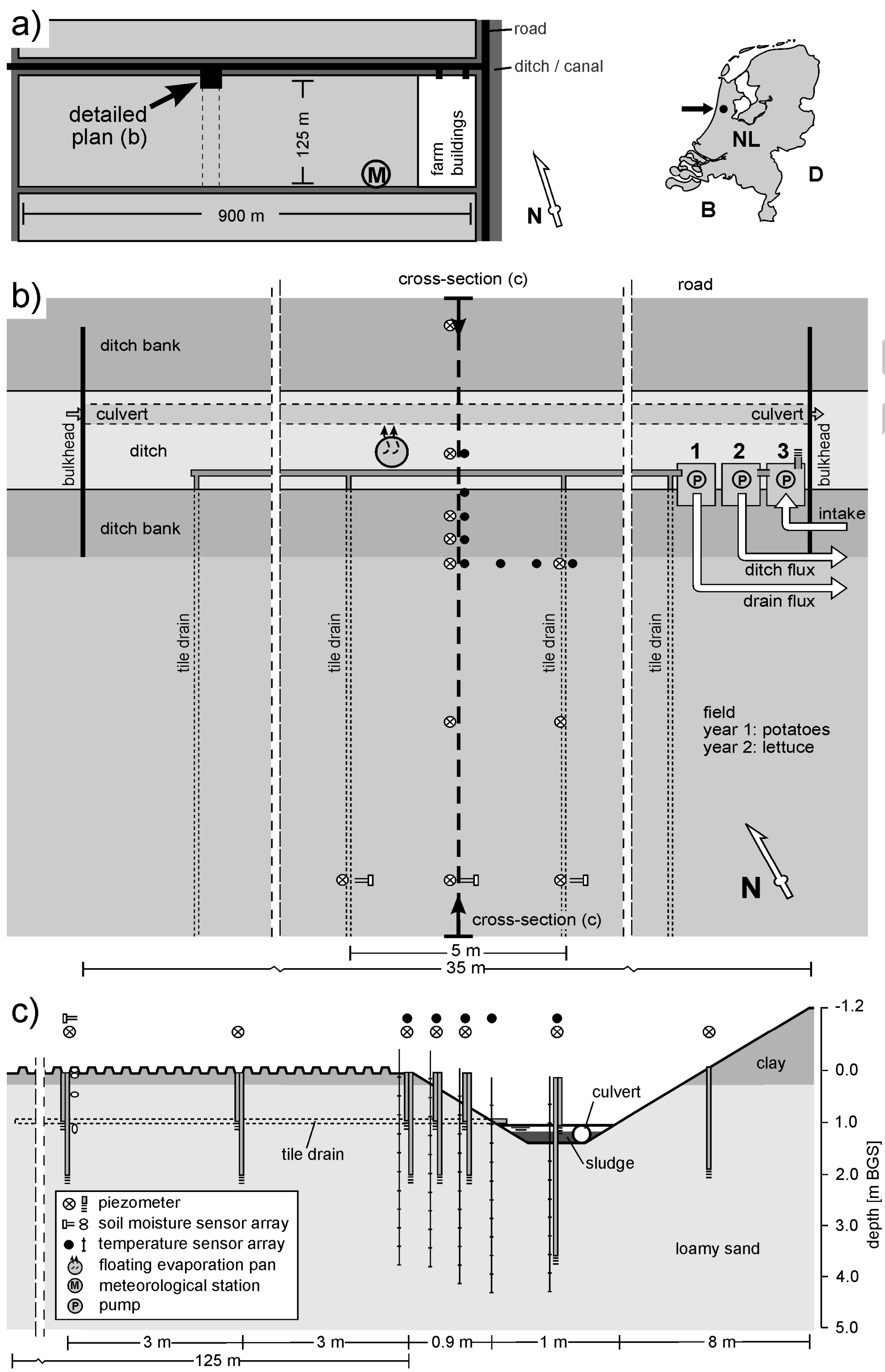

1094

1095 **Figure 1 Measurement setup and location of field site, with overview of field setup (a), measurement**

1096 **setup around ditch (b) and cross-sectional view of ditch measurement setup (c).**

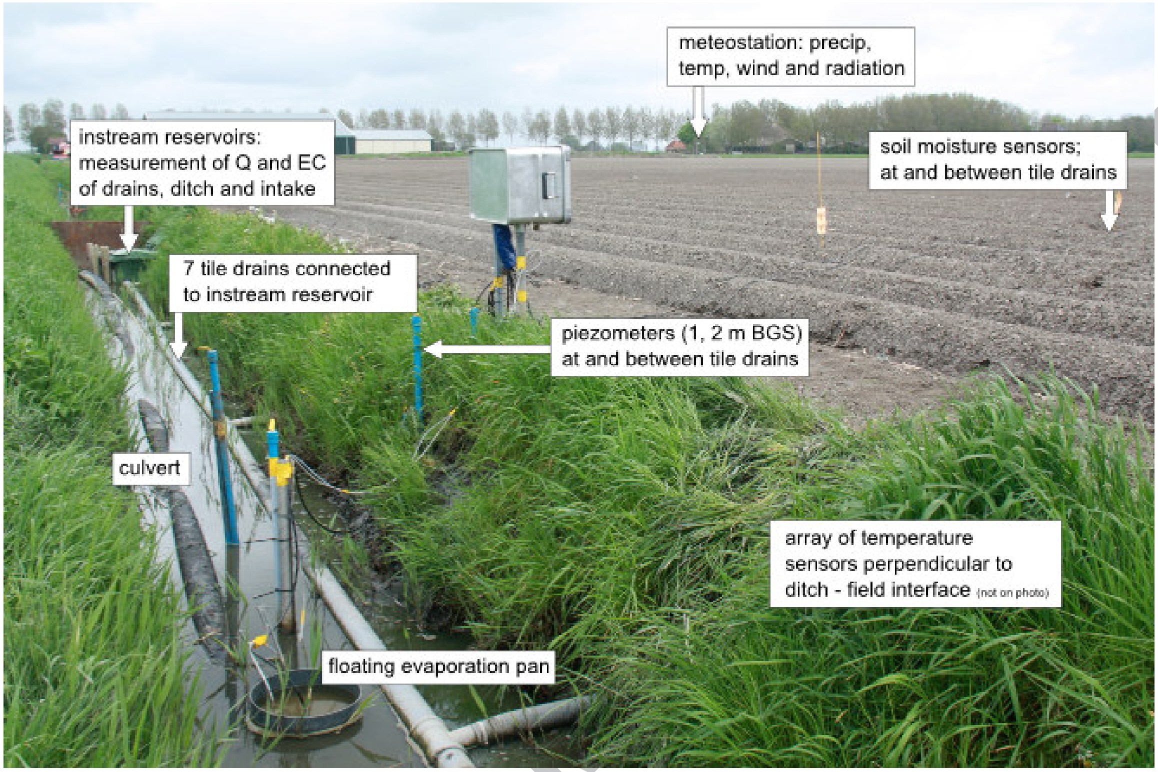

Figure 2: Measurement setup

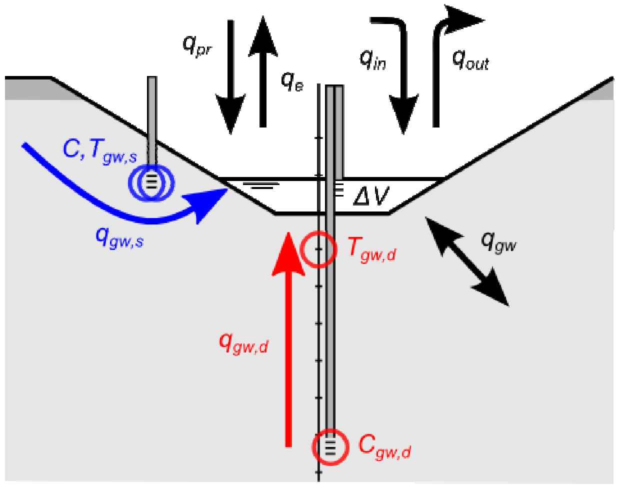

Figure 3: Schematic overview of fluxes (q_{pr} precipitation, q_e evaporation, q_{in} ditch intake flux, q_{out} ditch discharge, q_{gw} groundwater in- / exfiltration) entering and exiting the ditch (black lines). Coloured lines represent the separation of q_{gw} in a shallow ($q_{gw,s}$) and a deep ($q_{gw,d}$) component, and measurement locations of *C* (concentration, TDS) and *T* (temperature) of these fluxes; *ΔV* is volume change of ditch water.

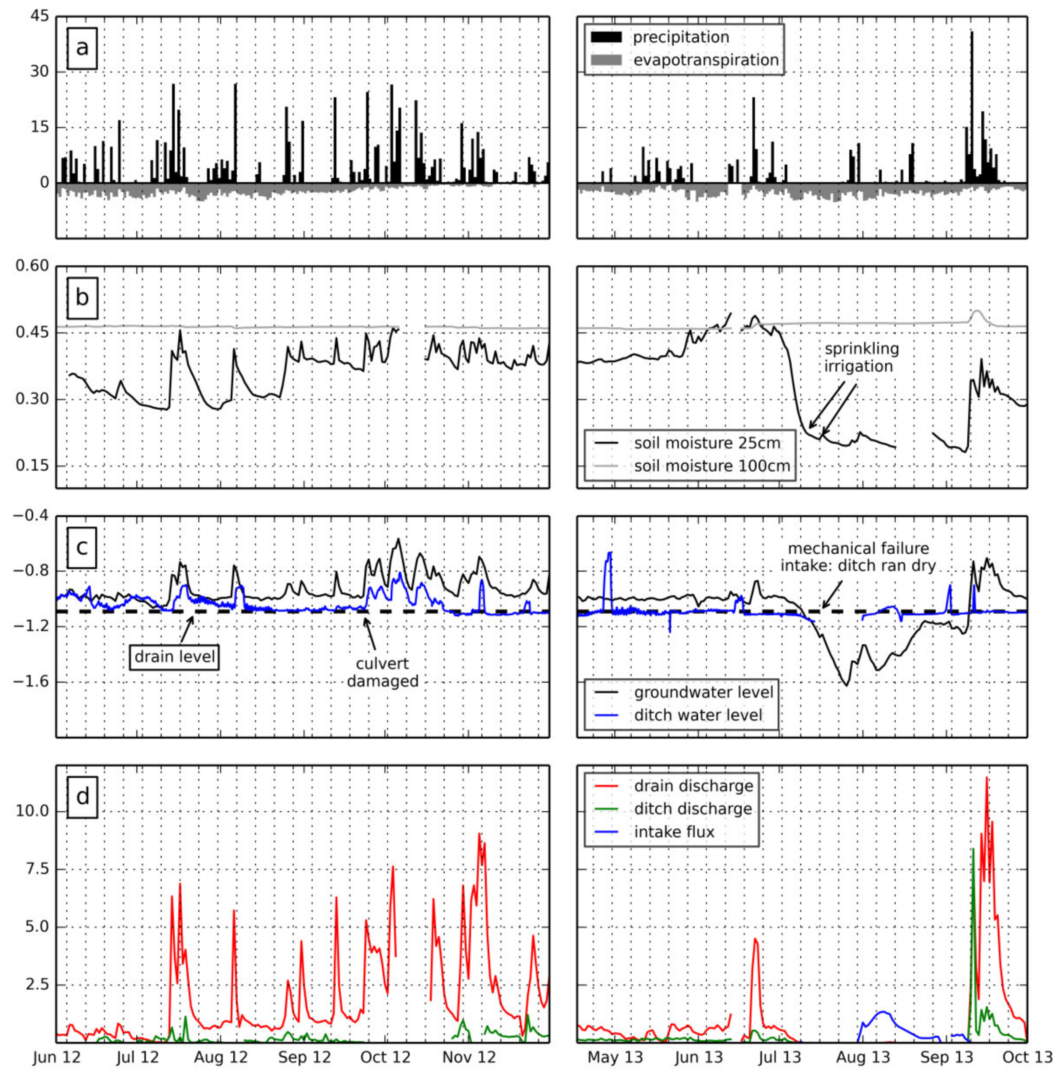

Figure 4: Precipitation and evapotranspiration (mm/d) (a), volumetric water content soil (-) (b), ground- and surface water level (m BGS) (c) and discharge (mm/d) (d) during measurement periods. Missing data are due to system malfunction (filter clogging, power failure).

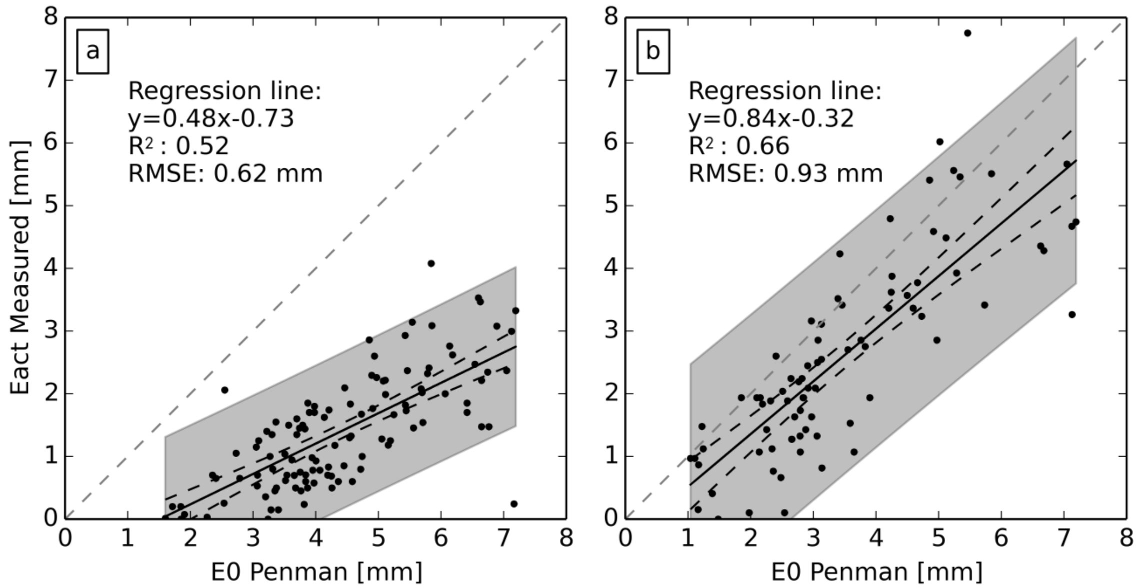

1116

1117 **Figure 5: Measured and calculated open water evaporation values, in the instrumented ditch (a), and**
1118 **the wider and deeper ditch on the other side of the field (b). Solid lines denote the linear regression**
1119 **lines, dashed lines and shaded areas represent the 95% confidence interval of the regression and the 95%**
1120 **prediction interval respectively, the 1:1 line is indicated in dashed grey.**

1121

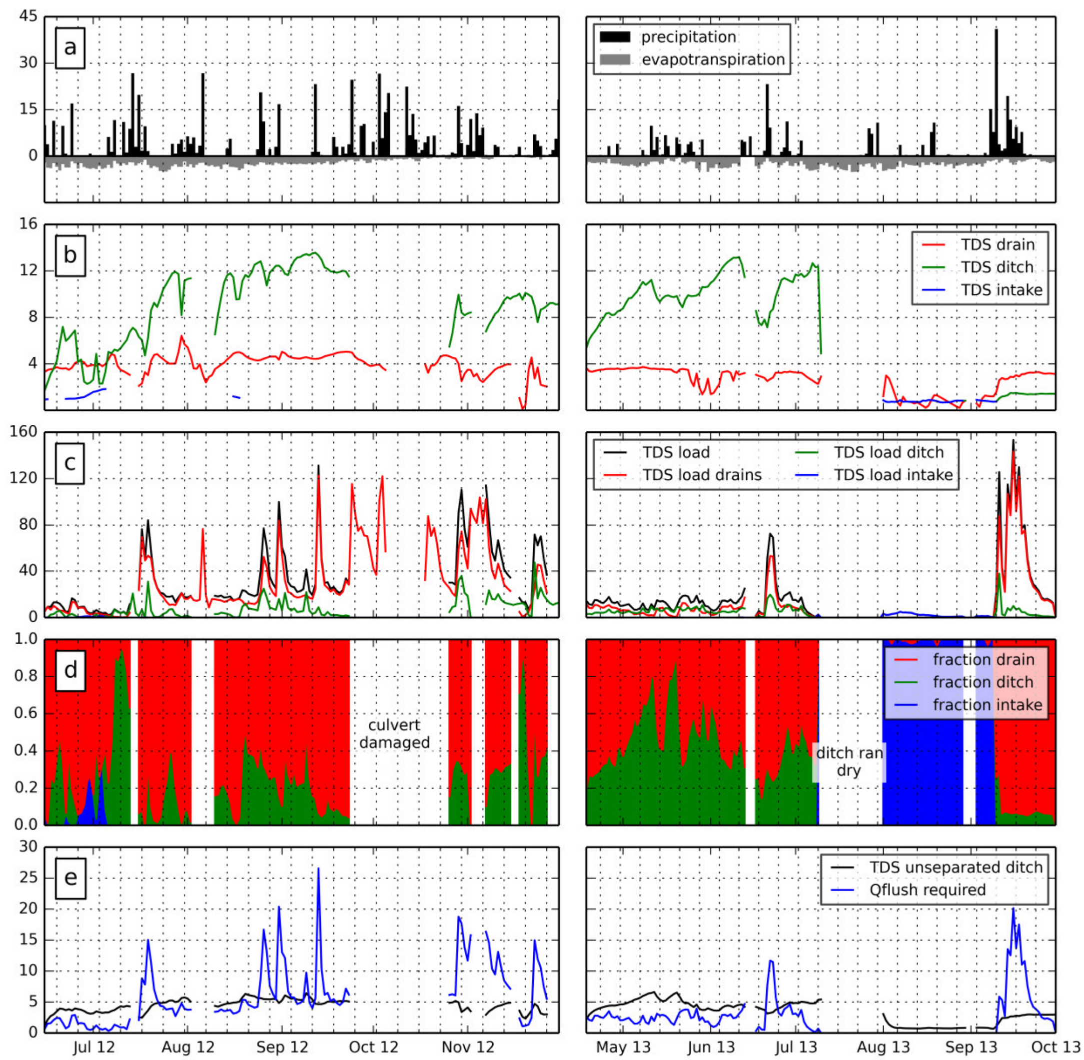

1122

1123 **Figure 6: TDS variation and contribution to salinity load to surface water, with a) precipitation and**
1124 **evapotranspiration (mm/d), b) TDS of tile drains, ditch and intake (g/L), c) TDS load of tile drains, ditch**
1125 **and intake (kg/d), d) fraction of tile drains, ditch and intake in TDS load (-), and e) calculated TDS of**
1126 **ditch if non-separated (g/L) and required flushing flux to keep surface water TDS at 1.5 g/L (mm/d).**

1127

1128

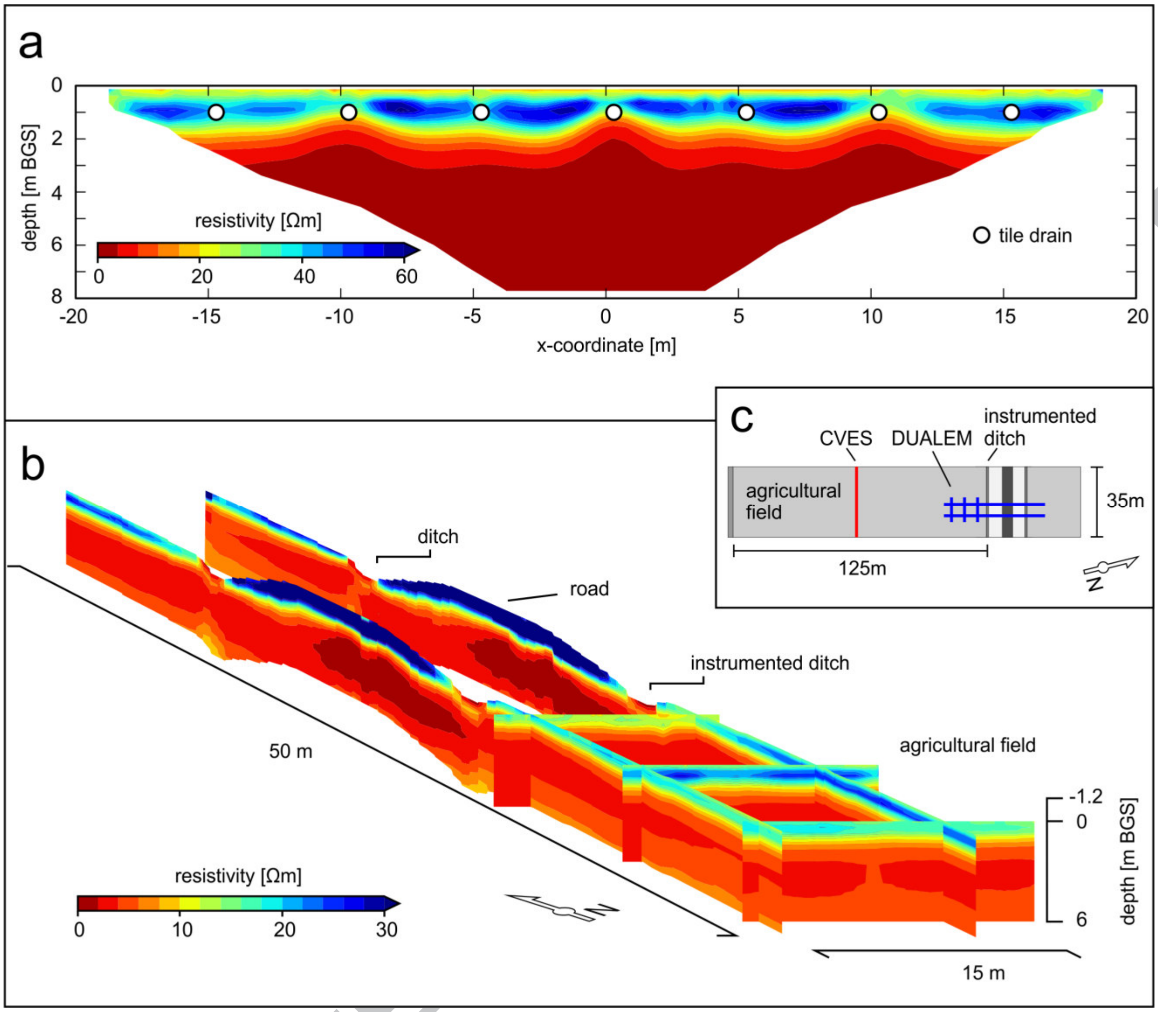

1129

1130 **Figure 7: Resistivity profiles measured by CVES (a) and DUALEM (b), locations in (c). Note the different**

1131 **resistivity scale between (a) and (b).**

1132

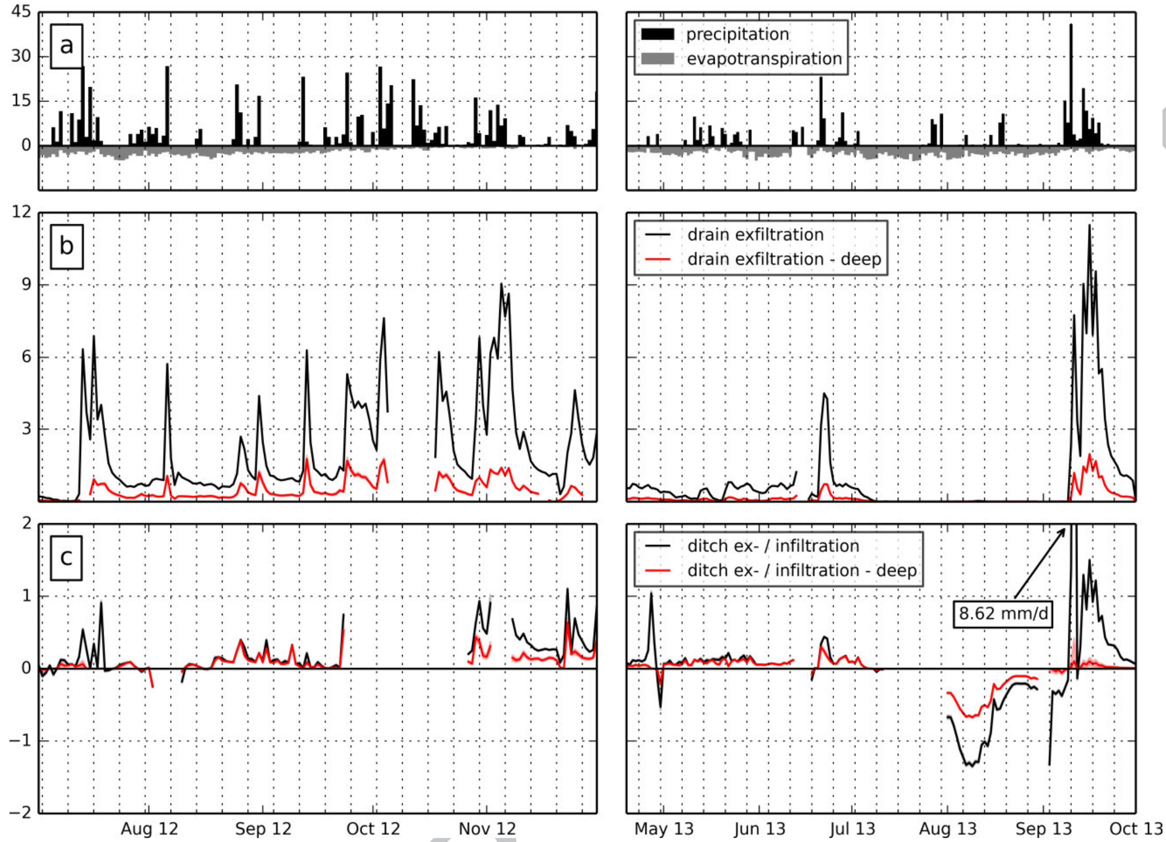

Figure 8: Flow path separation of drain and ditch exfiltration, with precipitation and evapotranspiration (mm/d) (a), drain exfiltration and deep groundwater contribution to drains (mm/d) (b) and ditch ex- and infiltration and deep flow path contribution (mm/d) (c). Missing data periods are caused by power failures or filter clogging. (Thin) shaded area in (b) around the deep groundwater contribution is based on min – max values for both deep groundwater and rainwater TDS, shaded areas in (c) span the Monte Carlo 25 – 75 percentile values, lines denote the median values.

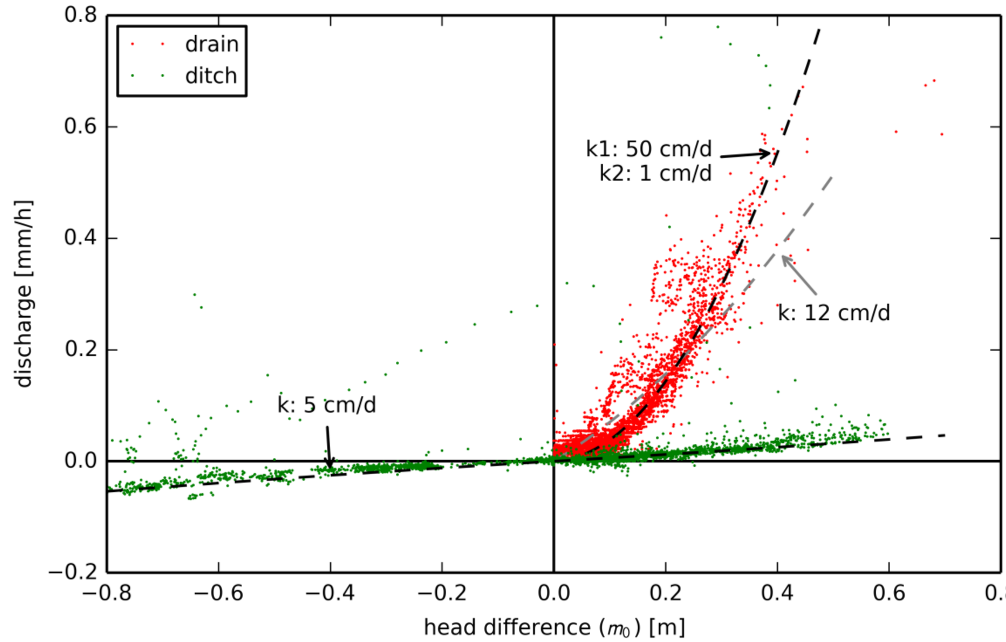

Figure 9: Discharge versus head difference for drain exfiltration and ditch ex-/infiltration. Dashed lines are Hooghoudt equations (Eq. 7) fitted to the data with denoted hydraulic conductivities.

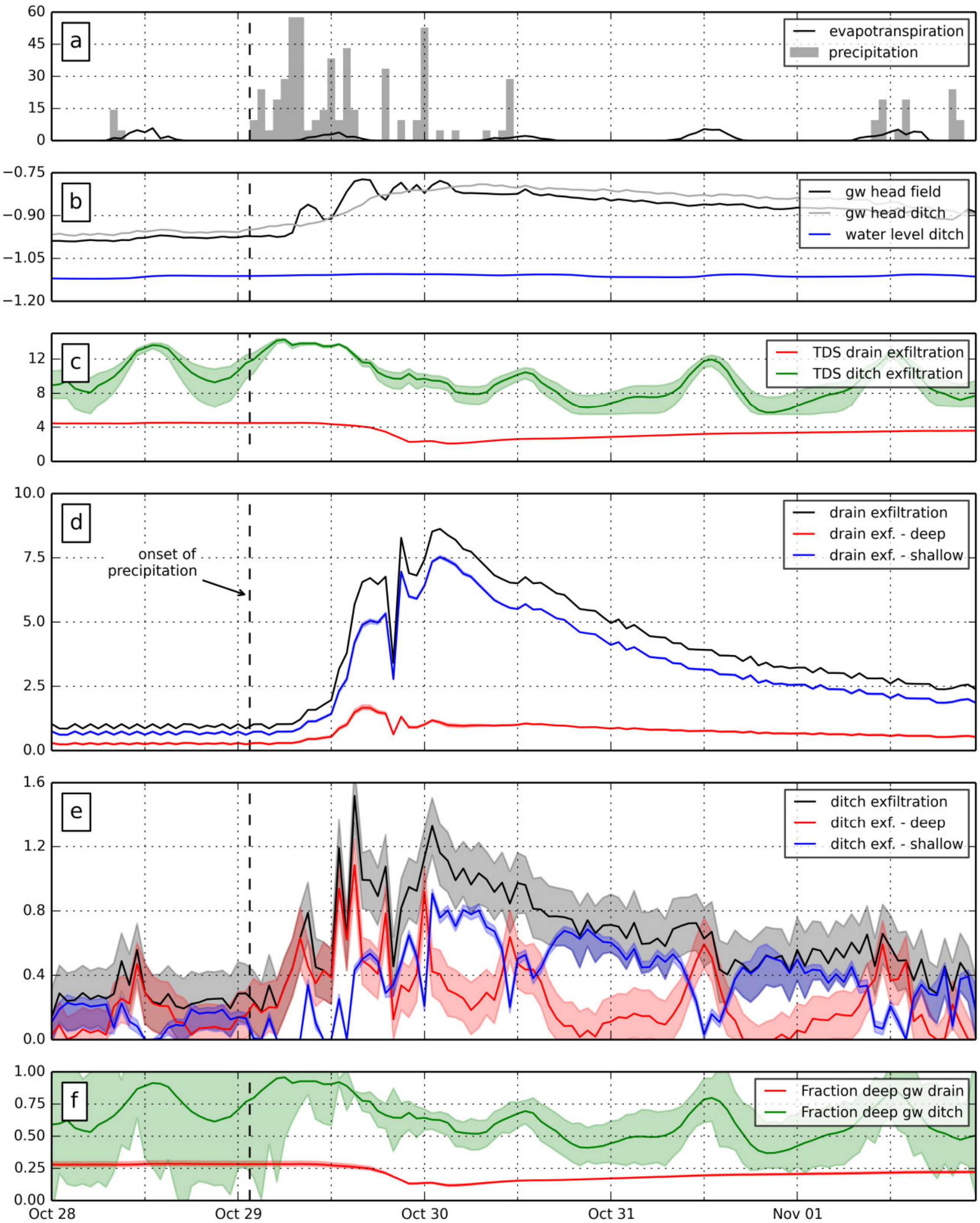

1146

1147 **Figure 10: Precipitation event Oct 29 2012, with a) precipitation and evapotranspiration (mm/d), b)**
1148 **groundwater and ditch surface water levels during the event (m BGS), c) TDS of drain and ditch**
1149 **exfiltration (g/L), d) total exfiltration and contribution of deep groundwater to tile drains (mm/d), e)**
1150 **total exfiltration and contribution of deep groundwater to ditch (mm/d) and f) fraction of deep**

1151 **groundwater in drain and ditch exfiltration. Shaded areas denote 25th and 75th percentile of Monte**

1152 **Carlo runs. Note that fluxes are in mm/d for consistency, but all data are hourly values.**

1153

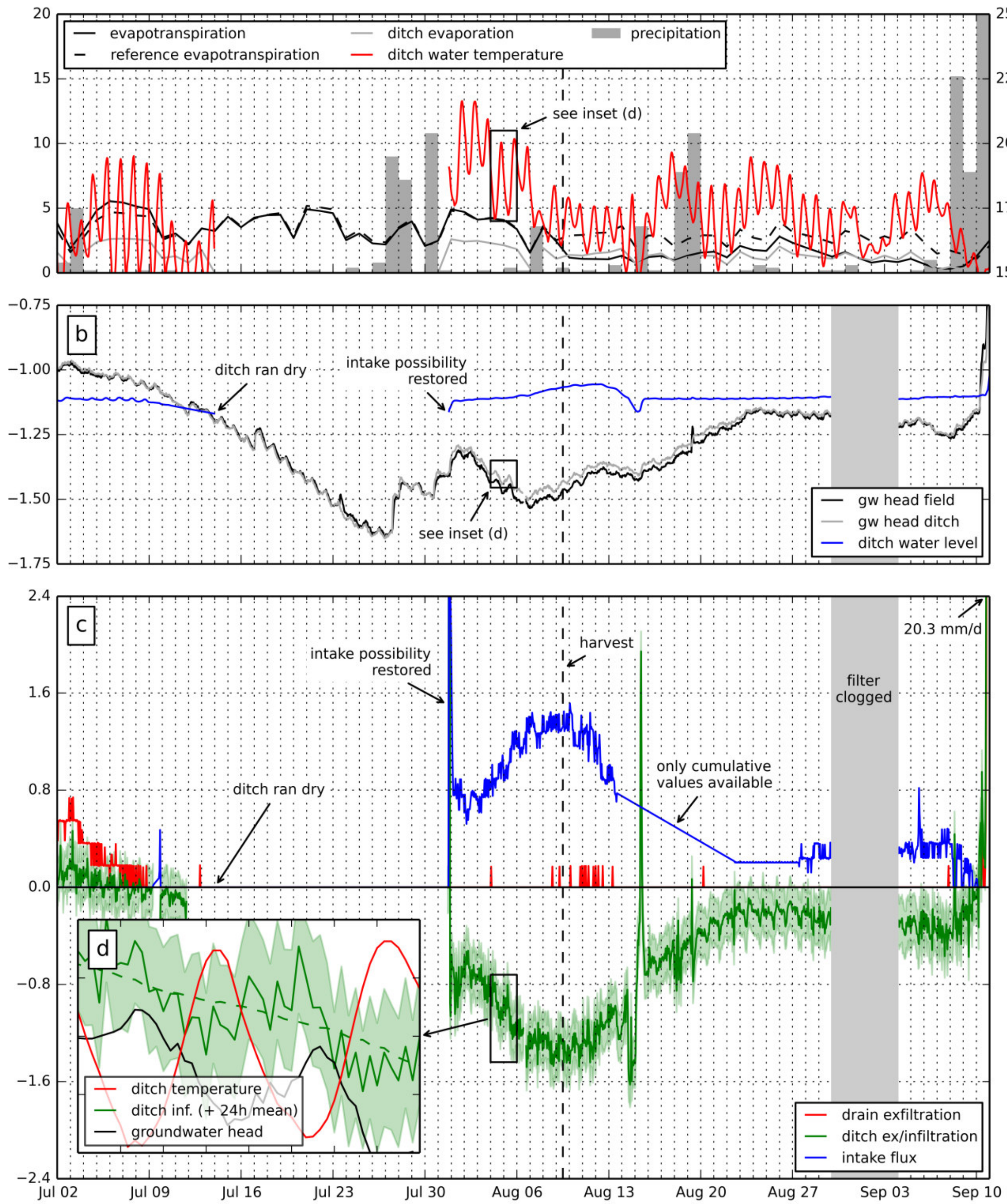

1154

1155 **Figure 11: Infiltration event Jul – Aug 2013, with a) precipitation (mm/d), evapotranspiration (mm/d)**

1156 **and ditch water temperature (°C, secondary y-axis), b) groundwater and ditch surface water levels (m**

BGS), c) ex- / infiltration to and from ditch, intake flux and drain exfiltration (mm/d), and d) ditch water temperature, groundwater head ditch and ditch infiltration between Aug 4 and Aug 6. Ditch ran dry from Jul 14 to Jul 31. Shaded area around ditch ex- / infiltration denotes 25th and 75th percentile of Monte Carlo runs. Note that fluxes are in mm/d for consistency, but all data are hourly values.

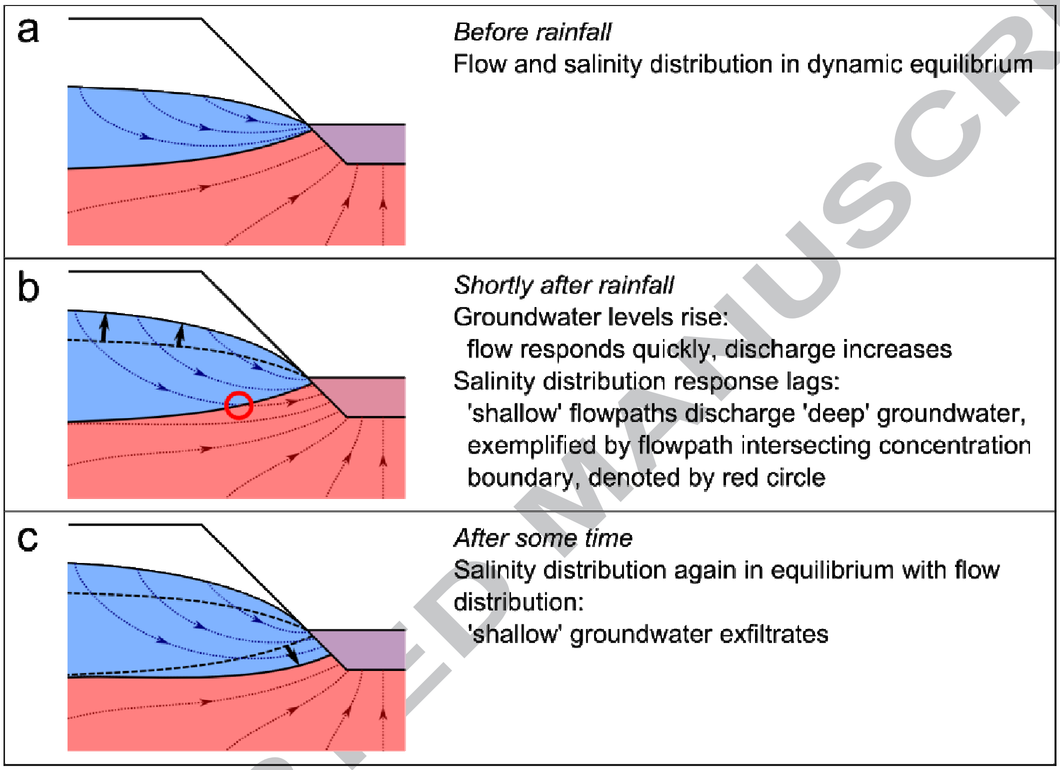

Figure 12: Conceptual representation of timing of shallow and deep exfiltration to ditch. Dotted lines depict the flow path distribution, thick arrows the movement of the fresh-saline interface. Note that the drawn sharp interface is in fact a continuum between fresh and saline groundwater (De Louw et al., 2013)**, and timescales of discharge events are too short to reach equilibrium conditions. Red circle in b) denotes 'shallow' flow path intersecting concentration boundary, thereby transporting 'deep' groundwater.**

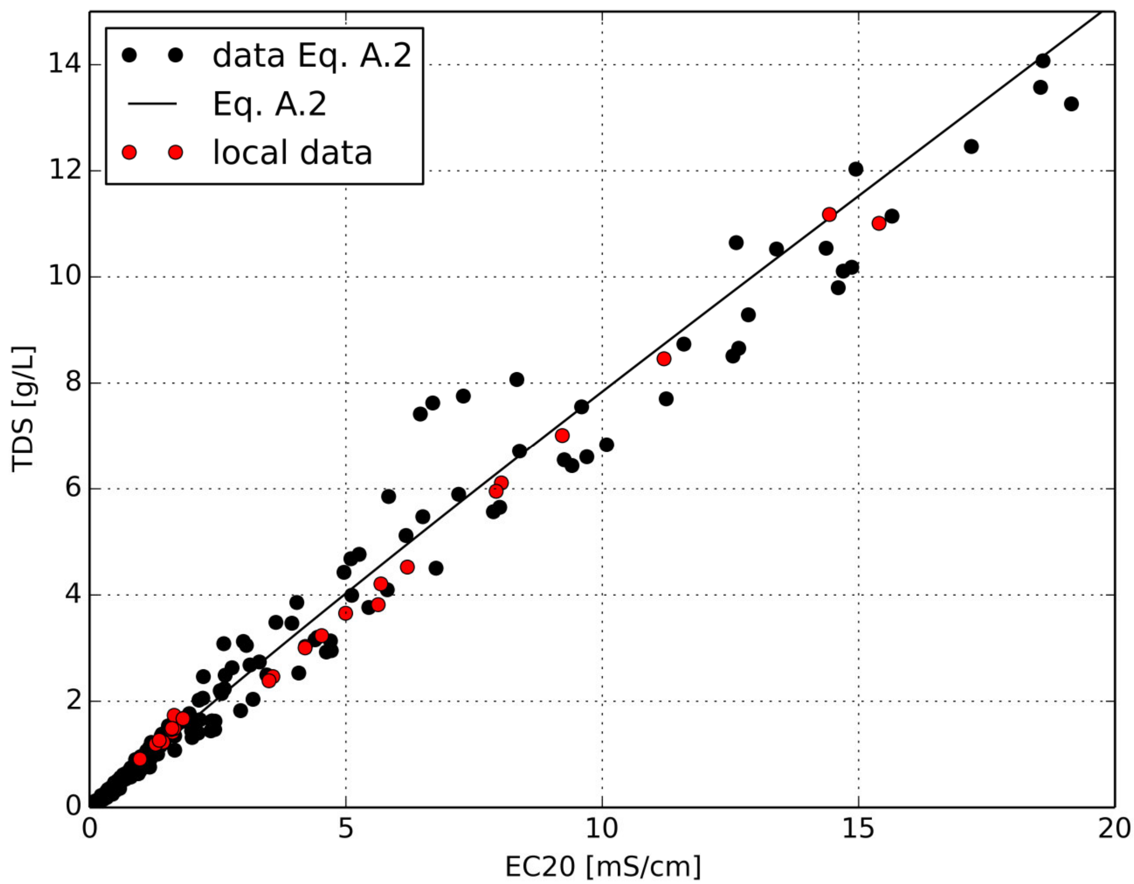

Figure A.1: EC20 – TDS relation of local samples of shallow groundwater plotted against Eq. A.2 and the original dataset used for its derivation (adapted from Stuyfzand (2014))

Figure 13 Measurement setup and location of field site, with overview of field setup (a), measurement setup around ditch (b) and cross-sectional view of ditch measurement setup (c).

Figure 14: Measurement setup

Figure 15: Schematic overview of fluxes (q_{pr} precipitation, q_e evaporation, q_{in} ditch intake flux, q_{out} ditch discharge, q_{gw} groundwater in- / exfiltration) entering and exiting the ditch (black lines). Coloured lines represent the separation of q_{gw} in a shallow ($q_{gw,s}$) and a deep ($q_{gw,d}$) component, and measurement locations of C (concentration, TDS) and T (temperature) of these fluxes; ΔV is volume change of ditch water.

Figure 16: Precipitation and evapotranspiration (mm/d) (a), volumetric water content soil (-) (b), ground- and surface water level (m BGS) (c) and discharge (mm/d) (d) during measurement periods. Missing data are due to system malfunction (filter clogging, power failure).

Figure 17: Measured and calculated open water evaporation values, in the instrumented ditch (a), and the wider and deeper ditch on the other side of the field (b). Solid lines denote the linear regression lines, dashed lines and shaded areas represent the 95% confidence interval of the regression and the 95% prediction interval respectively, the 1:1 line is indicated in dashed grey.

Figure 18: TDS variation and contribution to salinity load to surface water, with a) precipitation and evapotranspiration (mm/d), b) TDS of tile drains, ditch and intake (g/L), c) TDS load of tile drains, ditch and intake (kg/d), d) fraction of tile drains, ditch and intake in TDS load (-), and e) calculated TDS of ditch if non-separated (g/L) and required flushing flux to keep surface water TDS at 1.5 g/L (mm/d).

Figure 19: Resistivity profiles measured by CVES (a) and DUALEM (b), locations in (c). Note the different resistivity scale between (a) and (b).

Figure 20: Flow path separation of drain and ditch exfiltration, with precipitation and evapotranspiration (mm/d) (a), drain exfiltration and deep groundwater contribution to drains (mm/d) (b) and ditch ex- and infiltration and deep flow path contribution (mm/d) (c). Missing data periods are caused by power failures or filter clogging. (Thin) shaded area in (b) around the deep groundwater contribution is based on min – max values for both deep groundwater and rainwater TDS, shaded areas in (c) span the Monte Carlo 25 – 75 percentile values, lines denote the median values.

Figure 21: Discharge versus head difference for drain exfiltration and ditch ex-/infiltration. Dashed lines are Hooghoudt equations (Eq. 7) fitted to the data with denoted hydraulic conductivities.

Figure 22: Precipitation event Oct 29 2012, with a) precipitation and evapotranspiration (mm/d), b) groundwater and ditch surface water levels during the event (m BGS), c) TDS of drain and ditch exfiltration (g/L), d) total exfiltration and contribution of deep groundwater to tile drains (mm/d), e) total exfiltration and contribution of deep groundwater to ditch (mm/d) and f) fraction of deep groundwater in drain and ditch exfiltration. Shaded areas denote 25th and 75th percentile of Monte Carlo runs. Note that fluxes are in mm/d for consistency, but all data are hourly values.

Figure 23: Infiltration event Jul – Aug 2013, with a) precipitation (mm/d), evapotranspiration (mm/d) and ditch water temperature (°C, secondary y-axis), b) groundwater and ditch surface water levels (m BGS), c) ex- / infiltration to and from ditch, intake flux and drain exfiltration (mm/d), and d) ditch water temperature, groundwater head ditch and ditch infiltration between Aug 4 and Aug 6. Ditch ran dry from Jul 14 to Jul 31. Shaded area around ditch ex- / infiltration denotes 25th and 75th percentile of Monte Carlo runs. Note that fluxes are in mm/d for consistency, but all data are hourly values.

Figure 24: Conceptual representation of timing of shallow and deep exfiltration to ditch. Dotted lines depict the flow path distribution, thick arrows the movement of the fresh-saline interface. Note that the drawn sharp interface is in fact a continuum between fresh and saline groundwater (De Louw et al., 2013)**, and timescales of discharge events are too short to reach equilibrium conditions. Red circle in b) denotes 'shallow' flow path intersecting concentration boundary, thereby transporting 'deep' groundwater.**

Figure A.1: EC20 – TDS relation of local samples of shallow groundwater plotted against Eq. A.2 and the original dataset used for its derivation (adapted from Stuyfzand (2014))